Table 3

FBN2 and *TCERG1L* gene expression changes in colon tumor samples from ONCOMINE database

Colon cancer	Sample no.	Median log2 ratioa		References
		TCERG1L	*FBN2*	
Adenomas				
Colon villous adenoma	17	−1.862	−1.078	Not published since 2005 (Bittner Group)
Carcinoma				
Colon adenocarcinoma	41	−1.41	−1.142	Kaiser et al. [18]
Colon mucinous adenocarcinoma	13	−1.454	−1.184	Kaiser et al. [18]
Colon adenocarcinoma	137	−0.698	−0.51	Jorissen et al. [19]
Colorectal adenocarcinoma	177	−1.465	−1.229	Smith et al. [20]
Colon adenocarcinoma	239	−1.121	−0.808	Not published since 2005 (Bittner Group)
Colon mucinous adenocarcinoma	42	−1.623	−0.794	Not published since 2005(Bittner Group)
Colorectal carcinoma	84	−1.459	−1.598	Watanabe et al. [21]

[a]log2 median-centered intensity which is array-based gene expression log-fold changes. Oncomine threshold by p value (<0.0001), fold change (>2)

Tumor Biol.
DOI 10.1007/s13277-011-0278-y

RESEARCH ARTICLE

Hypermethylation of Sox17 gene is useful as a molecular diagnostic application in early gastric cancer

Yoshichika Oishi · Yoshiyuki Watanabe · Yoshihito Yoshida · Yoshinori Sato · Tetsuya Hiraishi · Ritsuko Oikawa · Tadateru Maehata · Hiromu Suzuki · Minoru Toyota · Hirohumi Niwa · Michihiro Suzuki · Fumio Itoh

Received: 6 September 2011 / Accepted: 15 November 2011

Abstract Although minimal invasive treatment is widely accepted in the early stages of gastric cancer (GCa), we still do not have any appropriate risk markers to detect residual neoplasia and the potential for recurrence. We previously reported that aberrant DNA methylation is an early and frequent process in gastric carcinogenesis and could be useful for the detection of gastric neoplasia. Our goal is to find and identify some candidate genes, using genome-wide DNA methylation analysis, as a treatment marker for early gastric cancer (EGC). We performed methylated CpG island amplification microarray analysis using 12 gastric washes (six each of pre- and post-endoscopic treatment in each of the same patients). We finally focused on Sox17 gene. We examined the DNA methylation status of Sox17 in a validation set consisting of 128 wash samples (pre, 64; post, 64) at EGC. We next carried out functional studies to identify Sox17. Sox17 showed significant differential methylation between pre- and post-treatments in EGC patients (Sox17, $p<0.0001$). Moreover, treating GCa cells that lacked Sox17 expression with a methyltransferase inhibitor, 5-aza-2′-deoxycytidine, restored the gene's expression. Additionally, the introduction of exogenous Sox17 into silenced cells suppressed colony formation. Gastric wash-based DNA methylation analysis could be useful for early detection of recurrence following endoscopic resection in EGC patients. Our data suggest that the silencing of Sox17 occurs frequently in EGC and may play a key role in the development and progression of the disease.

Keywords Sox17 · DNA methylation · Gastric cancer · Gastric washes

Yoshichika Oishi and Yoshiyuki Watanabe contributed equally to this work.

Electronic supplementary material The online version of this article (doi:10.1007/s13277-011-0278-y) contains supplementary material, which is available to authorized users.

Y. Oishi · Y. Watanabe (✉) · Y. Yoshida · Y. Sato · T. Hiraishi · R. Oikawa · T. Maehata · H. Niwa · M. Suzuki · F. Itoh
Division of Gastroenterology and Hepatology, Department of Internal Medicine, St. Marianna University School of Medicine, 2-16-1, Sugao, Miyamaeku, Kawasaki, Kanagawa 216-8511, Japan
e-mail: ponponta@marianna-u.ac.jp

Y. Watanabe · M. Toyota
Department of Biochemistry, Sapporo Medical University, Sapporo, Japan

H. Suzuki
First Department of Internal Medicine, Sapporo Medical University, Sapporo, Japan

Y. Watanabe
Department of Internal Medicine, Kawasaki Rinko General Hospital, Kawasaki, Japan

Abbreviations

GCa	Gastric cancer
EGC	Early gastric cancer
5-aza-dC	5-aza-2′-Deoxycytidine
Sox17	SRY (sex determining region Y)-box 17
MCAM	Methylated CpG island amplification microarray
ER	Endoscopic resection

Introduction

Gastric cancer (GCa) is the second leading cause of cancer death in the world. Its prognosis is determined by clinical

Published online: 08 December 2011

staging at diagnosis and treatment [1–3]. Diagnostic tools such as gastrointestinal endoscopy followed by pathological analysis and/or fluoroscopy have proven useful; however, the mortality rate has remained high throughout the world. The sensitivity and specificity of gastrointestinal (GI) endoscopy is high, but its diagnostic accuracy depends on the technical skill of the endoscopist—especially with artificial stomachs which have been partially resected by endoscopic or surgical treatment. Endoscopic biopsy is a topical procedure whereby only a small portion of abnormal tissue is removed. It can be difficult to determine which tissue layer to remove, thus occasionally leading to a misdiagnosis. Moreover, GI endoscopy is neither comfortable nor risk-free for patients, and it is associated with frequent morbidity. Furthermore, gastric cancer is more prevalent among elderly patients, who are likely to be taking medications such as antiplatelet or anticoagulant drugs, which further complicate the procedure.

The need for less invasive and more efficient diagnostic tools has led to a search for GCa antigens [4, 5]. However, we now know that common biomarkers such as CEA are not found frequently enough to yield high specificity or sensitivity assays. Molecular markers that distinguish benign from clinically silent malignant diseases are needed to reduce the number of unnecessary endoscopic biopsies and to improve detection of gastric dysplasia and gastric cancer at an early stage.

Endoscopists obtain gastric washes for analysis by washing around the stomach mucosa with a saline solution during routine endoscopic examination. Given that an abundant amount of cells are exfoliated into the washes and undamaged DNA recovered from the washes can be assayed with sensitive and quantitative techniques, there is a strong biological rationale to pursue this emerging technology [6].

Cytosine DNA methylation is an important epigenetic change which leads to the recruitment of transcription repressors and chromatin changes. During the development and progression of GCa, many genes are silenced by aberrant methylation of CpG islands, which are CpG dinucleotide-rich areas located within the promoters of approximately 60% of human genes [7]. Aberrant DNA methylation occurs more frequently than mutations in GCa [8–14]. Studies have detected cancer-specific DNA methylation in stool, blood plasma, urine, and pancreatic juice in several different cancers [15, 16]. Furthermore, concordant promoter hypermethylation of multiple genes, which is described as the "CpG island methylator phenotype", has been found in both gastric and colorectal carcinomas [17–22]. Therefore, these methylation markers could be useful for detecting field cancerization in this disease [23–25].

Recently, methylated CpG island amplification microarray (MCAM)-based genome-wide DNA methylation profiles have been available for analyzing primary neoplasms [26–30]. Although some candidate genes have been reported to undergo alterations in DNA methylation in GCa, such known genes are still limited for early gastric cancer (EGC) [18, 31–39]. We reported that gastric wash-based methylation analysis is useful for the detection of primary gastric neoplasia [6]. We hypothesized that gastric wash-based genome-wide methylation analysis could potentially be useful for selecting candidate genes in EGC. Additionally, gastric washes include large amounts of DNA recovered from cells on the surface of the stomach, making it simple to collect DNAs from patients endoscopically both pre- and post-minimal surgery treatment such as endoscopic resection (ER) [40, 41]. Comparing DNA methylation levels in each of the patients pre- and post-treatment is significant, as the selection of non-biased (i.e., aging, chronic inflammations, and *Helicobacter pylori* infections) EGC-specific genes, with alterations in DNA methylation, may become easier. Our goal is to find and identify some candidate genes as a treatment marker using genome-wide DNA methylation analysis for EGC.

Materials and methods

Cell lines

Seven GCa cell lines (MKN1, MKN7, MKN45, MKN74, NUGC3, KatoIII, and AZ521) were obtained from the American Type Culture Collection (Manassas, VA, USA) and the Japanese Collection of Research Bioresources (Tokyo, Japan). All cell lines were maintained in appropriate media containing 10% fetal bovine serum in plastic tissue culture plates.

Patient characteristics

Twelve test sets and 128 validation sets obtained from 140 gastric washes were collected from patients who underwent endoscopic resection for EGC at St. Marianna University School of Medicine Hospital (Kanagawa, Japan) from March 2005 to February 2010. In addition to the tumor samples, non-neoplastic gastric washes were collected from 32 age-matched patients who underwent endoscopic examination and were diagnosed with gastritis (Table 1). The study was conducted in accordance with all rules and regulations of the St. Marianna University School of Medicine Institutional Review Board (#1498), and informed consent was obtained from each patient.

Sample collection of gastric washes

To obtain gastric washes, patients were required to swallow a liquid solution (100 ml of water containing 80 mg of

Table 1 Clinical features of patients (cancer n=70, non-neoplastic n=32)

	Test set	Validation set			
	n=6	n=64	Average	Sox17 gene methylation (%)	p value
Age (n=70)			71.3±8.4		p=0.70
Male (n=50)	3	47	70.2±8.3	20.2±9.8	
Female (n=20)	3	17	74.4±8.0	22.0±11.2	
Endoscopic appearance					p=0.67
Polypoid	0	5		18.9±7.6	
Slightly elevated	6	29		20.4±9.3	
Flat	0	1		11.5±0.0	
Slightly depressed	0	29		21.5±11.5	
Histology (adenocarcinoma)					p=0.66
Well differentiated	6	44		20.3±10.1	
Moderately differentiated	0	20		21.4±10.4	
Stage					N/A
I	6	64		20.6±10.1	
II/III/IV	0	0		N/A	
Helicobacter pylori infection					p=0.76
Positive	3	43		20.7±10.5	
Negative	3	21		20.6±9.7	
Locations (stomach)					p=0.35
Upper body	0	11		17.6±7.8	
Middle/lower body	6	53		21.3±10.5	
Atrophy					p=0.80
Closed type	0	18		20.4±10.5	
Open type	6	46		20.8±10.1	
Intestinal metaplasia					p=0.23
Positive	6	54		21.3±10.5	
Negative	0	10		17.1±7.6	
Tumor size (square measure)			341.3±611.0		p=0.51
<341.3	6	48	108.4±96.9	20.9±10.1	
□341.3	0	16	1,040.0±919.1	20.0±10.6	
Control set					
Gastritis	0	32		13.6±6.8	

dimethylpolysiloxane [Gascon: Kissei Pharmaceutical Co., Ltd., Matsumoto, Japan], 1 g of sodium bicarbonate, and 20,000 U of pronase [Pronase MS: Kaken Pharmaceutical Co., Ltd., Tokyo, Japan]) approximately 10 min prior to endoscopic examination. Gastric washes were aspirated through the suction channel of the endoscope into specimen collection containers (No. 16200BZZ00045: Nippon Sherwood, Tokyo, Japan). The containers were directly connected to the endoscope modulator, and the washes were vacuumed manually. The samples were then immediately centrifuged and the pellets were frozen at −80°C. DNA was extracted using the standard phenol–chloroform method. The concentration and quantity of all DNA extracted from gastric washes were measured using the NanoDrop spectrophotometer (ND-1000 Spectrophotometer; Nano Drop Technologies, Wilmington, DE, USA).

After the collection of gastric washes, biopsies were carried out using biopsy forceps (Radial Jaw: Boston Scientific Corp., Natick, MA, USA) under endoscopic guidance with a GIF-Q260 endoscope using the EVIS LUCERA system (Olympus, Inc., Tokyo, Japan). Mucosal samples (approximately 5 mm in diameter each) of the gastric body and antrum were collected by biopsy. The rapid urease test was performed on two biopsy specimens using the PyloriTek test kit for *H. pylori* detection in the control set (Serim Research Corp. Elkhart, IN, USA). We used disposable sample collection tubes, connector tubes, and endoscopic devices. The endoscope

was washed with an automatic washing machine and disinfectant (DISOPA Solution 0.55%, Johnson and Johnson, Langhorne, PA, USA) after each patient according to the guidelines.

DNA and RNA preparation

DNA was extracted using the standard phenol–chloroform method from gastric cancer cell lines, gastric washes, and microdissected formalin-fixed paraffin-embedded (FFPE) tissues. Total RNA was extracted from the harvested cells using the Trizol (Invitrogen, Carlsbad, CA, USA) from gastric cancer cell lines. We also extracted an RNA sample from each of the 10 patients using Trizol (Invitrogen, Carlsbad, CA, USA) from endoscopically resected FFPE tissues in the validation set of EGC samples.

Methylated CpG island amplification microarray

For MCAM analysis, we analyzed 12 samples of primary EGC samples (six each of pre- and post-endoscopic resection in each of the same patients) using a test set. A detailed protocol of methylated CpG island amplification (MCA) was described previously [42]. We used a custom human promoter array (G4426A-02212; Agilent Technologies, Santa Clara, CA, USA) containing 36,579 probes corresponding to 9,021 unique genes. The probes on the array were selected to recognize *SmaI*/*XmaI* fragments, mostly around gene transcription start sites.

Five micrograms of genomic DNA was digested with 100 U of methylation-sensitive restriction endonuclease *SmaI* (New England Biolabs, Ipswich, MA, USA) for 24 h at 25°C, which cuts unmethylated DNA and leaves blunt ends (CCC/GGG). Subsequently, the DNA was digested with 20 U of methylation-insensitive restriction endonuclease *XmaI* for 6 h at 37°C, creating sticky ends (C/CCGGG). Five hundred milligrams of digested DNA was ligated using 50 μl of RMCA12 (5′-CCGGGCAGAAAG-3′) / RMCA24 (5′-CCACCGCCATCCGAGCCTTTCTGC-3′) primer and T4 DNA ligase (TaKaRa Bio Inc., Shiga, Japan) for 16 h at 16°C. After filling in the overhanging ends of the ligated DNA fragments at 72°C, the DNA was amplified at 95°C for 5 min followed by 25 cycles of 1 min at 95°C and 3 min at 77°C using 100 pmol of RMCA24 primer. MCA products were labeled with Cy5 (red) for DNA from pre-ER (both adjacent normal and tumor cells found in DNA from gastric washes) and Cy3 (green) for DNA from post-ER (only adjacent normal cells found in DNA from gastric washes) using a random primed Klenow polymerase reaction (Invitrogen) at 37°C for 3 h; 4×44 K human CpG island arrays were purchased from Agilent Technologies. Microarray protocols, including labeling, hybridization, and post-hybridization washing procedures, can be found at http://www.agilent.com/. Labeled samples were then hybridized to arrays in the presence of human Cot-1 DNA for 24 h at 65°C. After the washing procedures, arrays were scanned on an Agilent DNA Microarray Scanner and analyzed using Agilent Feature Extraction software (FE version 9.5.1.1, Agilent Technologies) at St. Marianna University School of Medicine. We used GeneSpring software (Agilent) for choosing candidate genes after normalization of the raw data.

Hierarchical clustering analysis

Unsupervised hierarchical clustering was done using an agglomerative hierarchical clustering algorithm following Lowess normalization. For specimen clustering, pairwise similarity measures among specimens were calculated using GeneSpring GX software based on the DNA methylation intensity measurements across all genes (version 11, Agilent Technologies).

DNA methylation analysis

Bisulfite polymerase chain reaction (PCR) was performed using an EpiTect Bisulfite Kit (QIAGEN, Valencia, CA, USA) according to the manufacturer's protocol. One microliter of bisulfite-treated DNA was used as a template. All of the primers used for amplifying promoter CpG DNA fragments of the gene are described in Supplementary Table 1. After PCR, the biotinylated strand was captured on steptavidin-coated beads (Amersham Bioscience, Uppsala, Sweden) and incubated with sequencing primers (Supplementary Table 1). Pyrosequencing quantitatively measures the methylation status of several CpG sites in a given promoter. These adjacent sites usually show highly concordant methylation. Therefore, the mean percentage of methylation at detected sites was used as a representative value for each gene promoter.

Trichostatin A and 5-aza-2′-deoxycytidine treatment of cells

To analyze restoration of each gene expression, cell lines were incubated for 96 h with 1 or 5 μM of 5-aza-2′-deoxycytidine (5-aza-dC) and/or 200 nM of trichostatin A (TSA) after which they were harvested and their RNA was extracted for further analysis.

Reverse transcription-polymerase chain reaction

First-strand cDNA was prepared by reverse transcription of 1-μg samples of total RNA using Superscript III Reverse Transcriptase (Invitrogen). Real-time quantitative reverse transcription-PCR was carried out using Taqman Gene Expression Assays [Sox17, Hs00751752_s1, and glyceraldehyde-3-phosphate dehydrogenase, Hs_00266705_g1 (Applied

Biosystems)] with an ABI 7500 Real-Time PCR System (Applied Biosystems) according to the manufacturer's instructions. SDS2.1 software (Applied Biosystems) was used to do comparative delta-Ct analysis. Glyceraldehyde-3-phosphate dehydrogenase served as an endogenous control.

Colony formation assays

Cells (0.5×10^5) were plated in 2-cm^2 culture dishes for 24 h before transfection with the expression vector Myc-DDK-tagged pCMV6-Sox17 expression vector or empty vector (RC220888 and PS100001, OriGene Technologies, Rockville, MD, USA) using 2 μl of Lipofectamine 2000 (Invitrogen) according to the manufacturer's instructions. After transfection, cells were preserved for 14 days in a medium containing 0.2 mg/ml G418 for MKN74, 0.6 mg/ml G418 for MKN45 and stained with Giemsa. The resultant colonies were then stained with crystal violet and cells were counted in triplicate cultures using NIH Image software. Western blotting was carried out using anti-Sox17 antibody (AF1924, R&D Systems, Minneapolis, MN, USA) and anti-DDK monoclonal antibody (TA50011, OriGene Technologies).

Statistical analysis

Methylation levels (percentage) were analyzed as a continuous variable for comparison of Sox17 genes. The mean and 95% confidential intervals were calculated for clinicopathologic features. The correlation of DNA methylation between gastric wash samples and formalin-fixed, paraffin-embedded tissues were analyzed using the Mann–Whitney test for continuous variables and $p<0.05$ was considered significant. All statistical analyses were performed using PRISM software for Windows, version 4 (GraphPad Prism, Inc., San Diego, CA, USA).

Results

Clinicopathologic characteristics of patients with EGC

A total of 140 gastric wash samples from 70 primary EGC patients were analyzed including 5 polypoid type, 35 (6+29) slightly elevated types, 1 flat type, and 29 slightly depressed types. The samples were analyzed histologically including 50 (6+44) well-differentiated adenocarcinoma and 20 moderately differentiated adenocarcinoma at the St. Marianna University School of Medicine (50 (3+47) men and 20 (3+17) women; average age, 71.3±8.4 years) (Table 1). All samples were reviewed by an expert gastrointestinal pathologist. Thirty of the 140 FFPE slides were obtained from the pathology archives of St. Marianna University School of Medicine. The 140 test samples and validation sets collected both included stage I, differentiated adenocarcinoma samples that are approved in standard ER therapy by The Japanese Gastric Cancer Association gastric cancer treatment guidelines [43]. A control set of non-neoplastic gastric washes from 32 age-matched patients who underwent endoscopic examination had gastritis (20 men and 12 women; average age, 70.1±4.2 years) (Table 1). Only one case was diagnosed to have residual cancer due to tumor cells found in the vertical margin of the resected specimen. Otherwise, we did not find any residual/recurrent disease, even in short-term follow-up.

Sox17 selected as a candidate gene for EGC detection by MCAM analysis

To compare the gastric wash-based global DNA methylation profiles of pre- and post-ER, we analyzed 12 test set samples from six patients (two samples/patients) using MCAM. A Cy5/Cy3 (pre-ER/post-ER) signal in excess of 1.0 (Log2 ratio) in MCAM was considered methylation-positive in three out of six cases (Fig. 1a). Eighteen probes (18/36,579) corresponding to 11 unique genes (11/9,021) were selected as candidate genes after calculations were made using GeneSpring GX software (version 11, Agilent Technologies) based on the DNA methylation intensity measurements (data not shown) (Fig. 1b). One of the probe is the Sox17 (SRY (sex determining region Y)-box 17) gene (Fig. 1b).

We next used Ingenuity Pathway Analysis to analyze all of the data (IPA version 8.0, Ingenuity Systems, Inc. Redwood, CA, USA). All of our microarray data (36,579 probes) were uploaded to IPA software to identify significantly related biological networks (31,125 probes were mapped). Functional classification of differentially methylated genes indicated that a cluster of genes were involved in EGC. In "biological functions from statistical analysis", these top ranking categories suggested interesting functions, such as "Cancer", "Developmental Disorder", and "Genetic Disorder" in the Disease and Disorders category; "Tissue Development", "Organ Development", "Organismal Development", and "Embryonic Development" in Physiological System Development and Function category; and "Molecular Mechanisms of Cancer", "Ephrin Receptor Signaling", "Human Embryonic Stem Cell Pluripotency", and "Wnt/β-catenin Signaling" in the Canonical Pathways category (Supplementary Table 2).

In the end, we focused on the Sox17 gene because it has a CpG island in its promoter region and is known to be associated with both "Cancer" and "Wnt/ β-catenin signaling pathway" in gastric neoplasia (Fig. 4a) [44]. We next made Sox17 pyrosequencing primer to confirming MCAM data using 12 test sets from the EGC samples. High concordance was observed between the methylation status of genes

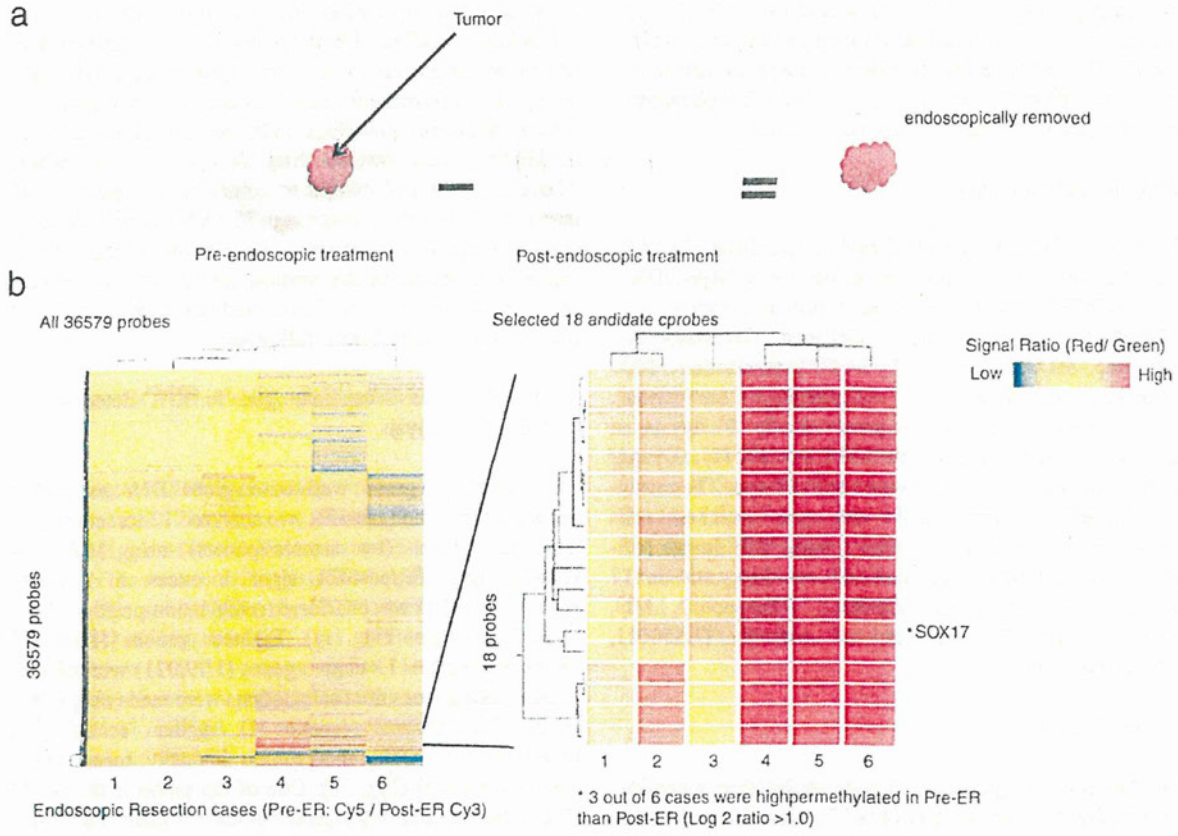

Fig. 1 Schema of our strategy and hierarchical clustering view. **a** We hypothesized that by comparing methylation levels of gastric washes from pre- and post-ER, we could more efficiently extract cancer-specific genes into the whole genome. **b** Sox17 gene was selected after hierarchical clustering by MCAM analysis. Three out of six patients were more highly methylated in pre-ER than in post-ER

identified by MCAM and pyrosequencing analysis in the test set ($p<0.05$, $r=0.81$).

Sox17 methylation may be useful as therapeutic marker for EGC

To further evaluate gastric wash-based DNA methylation of Sox17 genes, we next carried out quantitative bisulfite-pyrosequencing analysis using a larger panel of validation sets (128 samples). The Sox17 gene showed significantly higher methylation levels in pre-ER than post-ER (pre, $n=64$; post, $n=63$; excluded, $n=1$; Fig. 2, example in Fig. 3a). Pathological findings were diagnosed by an expert gastrointestinal pathologist. In the incomplete ER case, gastric wash-based Sox17 methylation showed no decrease in a level, and the pathologist also found that additional

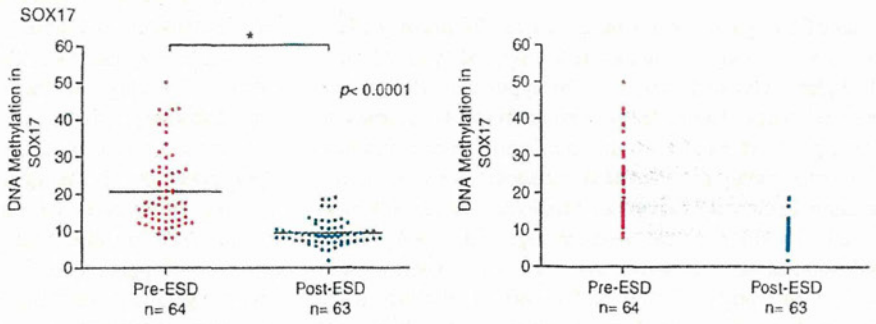

Fig. 2 DNA methylation in the validation set of EGC. Methylation levels of Sox17 measured by quantitative bisulfite pyrosequencing (pre- and post-ER). Results are of individual genes in the validation set. There is a significant difference in methylation levels between pre- and post-ER ($p<0.0001$)

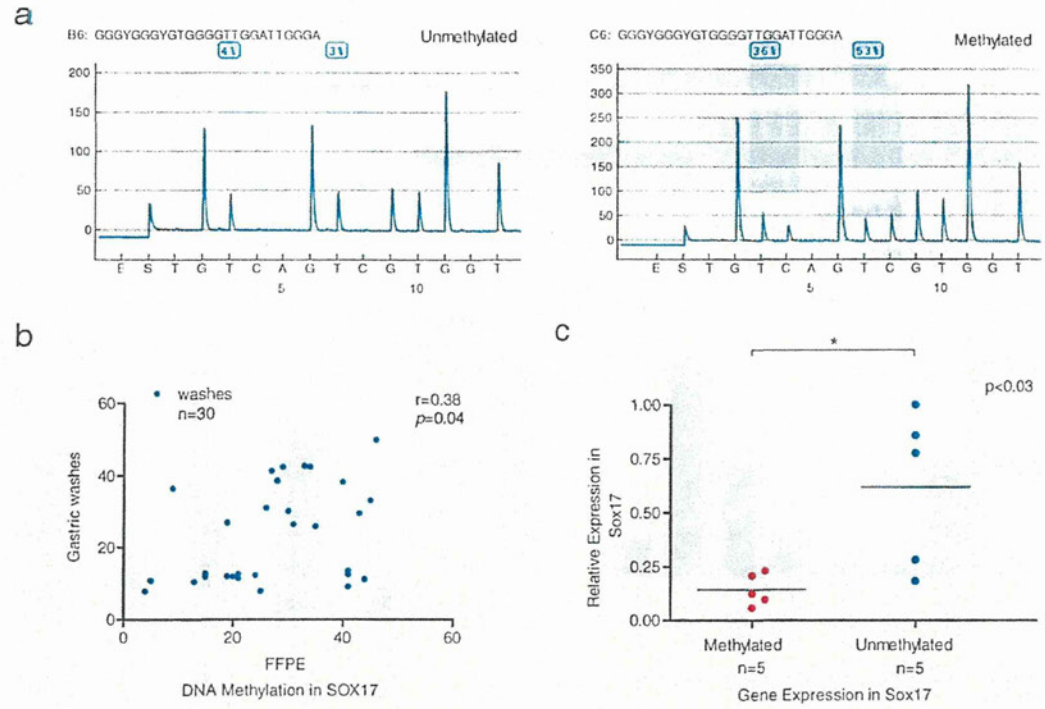

Fig. 3 Sox17 silenced by DNA methylation in EGC. **a** Gastric wash-based pyrogram of Sox17 gene in EGC (*left*, unmethylated; *right*, methylated). **b** Correlation of methylation levels between gastric washes and FFPE samples in the same patient. **c** Expression of Sox17 in EGC with or without DNA methylation ($p<0.03$). Real-time PCR was carried out using cDNA from extracted tumor tissue by laser capture microdissection after ER

resection resulted in the proof of residual cancer (Supplementary Fig. 1b, c). Additionally, to confirm correlations in Sox17 methylation levels between gastric washes and FFPE, 30 DNAs were extracted from 30 endoscopically resected FFPE tissues in conjunction with 30 wash samples in a validation set of 128 EGC patients are shown in Fig. 3b. Methylation levels of the Sox17 gene were approximately correlated between washes and FFPE by Spearman's correlation coefficient analysis ($r=0.38$, $p=0.04$) (Fig. 3b). To compare the Sox17 methylation levels between EGC and the gastritis samples (control samples), we analyzed the data using DNA from gastric washes of pre-ER ($n=64$)/post-ER ($n=63$) endoscopic treatment and 32 gastritis samples. The results show a significant difference between not only pre-ER and post-ER, but also between pre-ER and gastritis samples (Supplementary Fig. 1a). Interestingly, methylation levels were widely spread among gastritis samples, and we successfully divided them into two methylation groups based on the status of *H. pylori* infection (Supplementary Fig. 1a). On the other hand, there were no significant differences of Sox17 methylation levels between *H. pylori* positive and negative in EGC samples (gastric washes in pre-ER) (Table 1, Supplementary Fig. 1a).

Silencing of Sox17 associated with its promoter CpG island hypermethylation in gastric cancer cell lines

Human BLAT search sequence analysis of Sox17 5′ regulatory regions shows that there is a CpG island encompassing its transcription start site (UCSC Genome Bioinformatics Group, Santa Cruz, CA, USA). We designed primers for bisulfite-pyrosequencing analysis in a region downstream of the transcription start site (Fig. 4a). Although two of the gastric cell lines showed low methylation (MKN1, 57%; KatoIII, 35%), hypermethylation was detected in four of them (MKN7, 82%; MKN45, 92%; MKN74, 75%; AZ521, 86%). These four cell lines also expressed low levels of Sox17 (Fig. 4b). There were good correlations between DNA methylation levels and gene expression levels using 10 primary EGC samples (total RNA was extracted from 10 endoscopically resected FFPE tissues) (Fig. 3c).

To assess restoration of Sox17 expression, two hypermethylated cell lines (MKN45, MKN74) were incubated for 72 h with 1 and 5 μmol/l 5-aza-2′-deoxycytidine (Sigma-Aldrich, St. Louis, MO, USA), a methyltransferase inhibitor. The cells were then harvested, and total RNA was extracted for further analysis. Treating the two cell lines

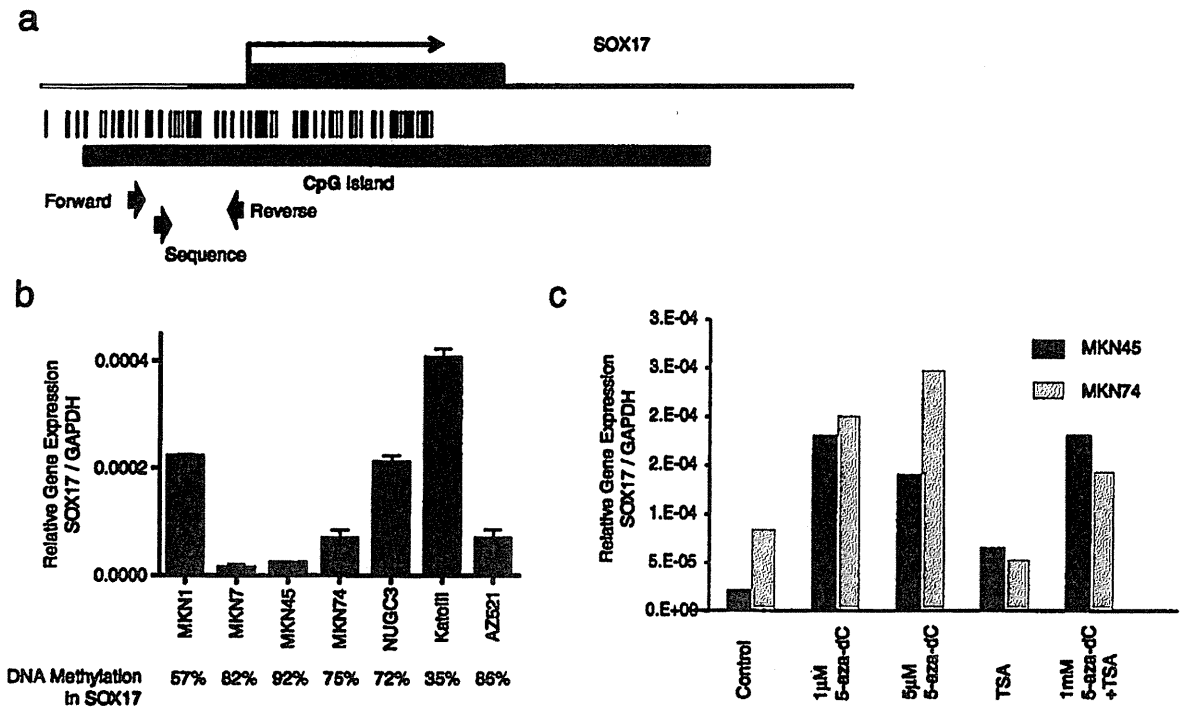

Fig. 4 CpG island of Sox17 and gene expressions. a Schema of the promoter region of Sox17 gene and CpG island (*black bar*). *Three arrows* were used to describe pyrosequencing primers for methylation analysis. b Relative expression levels of Sox17 gene in seven gastric cancer cell lines. Levels of Sox17 gene expression are normalized to glyceraldehyde-3-phosphate dehydrogenase (*GAPDH*). c Using real-time PCR, expression of Sox17 was analyzed in two gastric cancer cell lines (MKN74 and MKN45) that were highly methylated in Sox17. In two gastric cancer cell lines that expressed Sox17 at barely detectable levels, expression levels were restored after treatment with 5-aza-dC

(MKN45, MKN74) with the methyltransferase inhibitor 5-aza-dC, they showed hypermethylation in Sox17, and expression levels were restored (Fig. 4c).

Expression of exogenous Sox17 suppresses cell growth in gastric cancer cell lines

We next used colony formation assays to determine whether Sox17 has some potential for tumor suppressor activities (Fig. 5). When Sox17 was introduced to two gastric cancer cell lines that do not otherwise express the gene, there was a significant reduction in colony formation.

Discussion

Aberrant DNA methylation plays a crucial role in the development and progression of human cancers and is now recognized as a third mechanism by which inactivation of tumor suppressor genes occurs [45]. Aberrant CpG island hypermethylation is also frequently observed in chronic inflammation and precancerous lesions, which suggests that it is an early occurrence in tumorigenesis that could serve as a useful tumor marker [46, 47]. A strategy was put in place to compare methylation levels between tumor and adjacent normal site in order to select candidate genes that were specifically methylated in neoplasia. However, it is difficult to eliminate some hypermethylated genes that were associated with age and inflammations (e.g., chronic gastritis by *H. pylori*). Our gastric wash-based MCAM analysis is an innovative approach to evaluating the DNA in gastric washes of cancer patients before and after ER of EGC (pre-ER gastric washes include both the tumor site and normal site; post-ER gastric washes only include the normal site due to the curative removal of a tumor site by endoscopic treatment). In the present study, we successfully selected 11 candidate genes out of 9,021 genes by means of gastric wash-based MCAM analysis.

It was reported previously that DNA methylation of the region around the transcription start site of Sox17 is involved in silencing the gene in colorectal cancer cells [48]. Consistent with that report, we also found that gene silencing by Sox17 hypermethylation was seen in MKN74 and MKN45 of gastric cancer cell lines (Fig. 4). The molecular mechanism by which Sox17 suppresses cell growth remains unknown. However, Zhang et al. [48] reported that

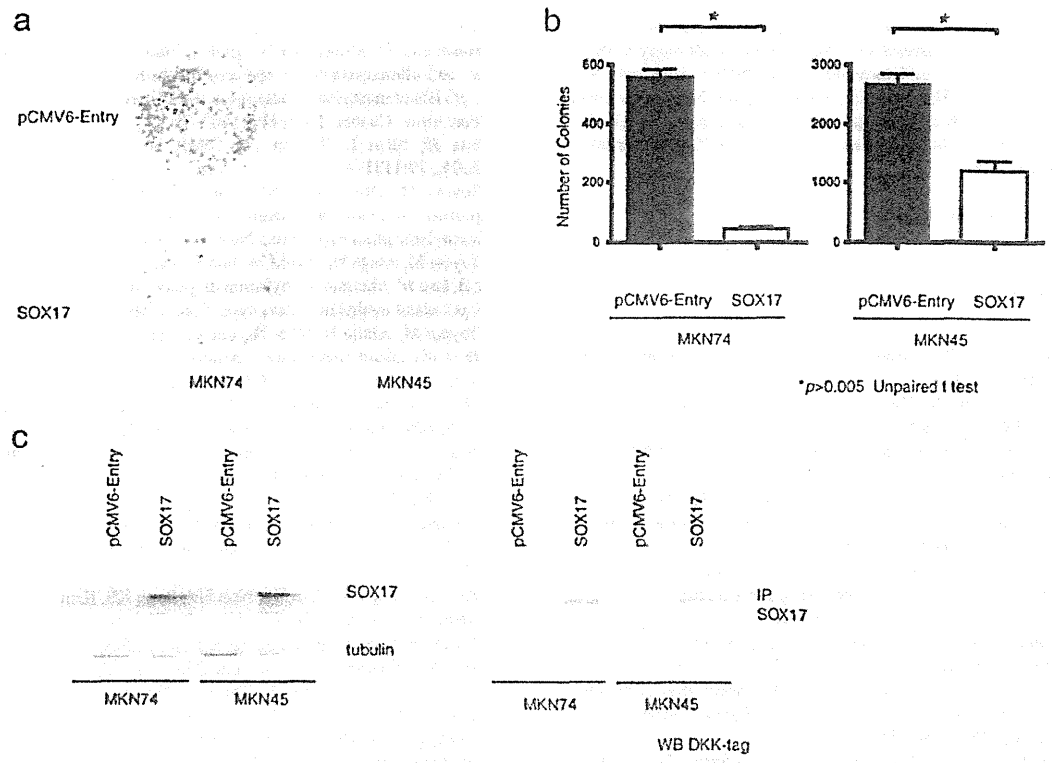

Fig. 5 Suppression of colorectal cancer cell growth by Sox17. a MKN74 and MKN45 cells were transfected in the presence of G418. b Cell counts were obtained 28 days after transfecting MKN74 and MKN45 with pCMV6 (empty vector) or pCMV6-Sox17 (Sox17). c To confirm Sox17 protein levels after transfection, we used pCMV6-Sox17 plasmid with DKK-tag by western blotting analysis

introducing Sox17 into colorectal cancer cells using a pcDNA3.1/V5-His vector represses β-catenin/TCF activity in cells, suggesting that the Sox17 is involved in the Wnt/β-catenin pathway. We also confirmed that introduction of exogenous Sox17 into silenced cells suppressed colony formation in gastric cancer cell lines (MKN74 and MKN45) (Fig. 5).

Molecular markers that distinguish benign from clinically silent malignant disease are needed to reduce the number of unnecessary endoscopic biopsies and to improve detection of gastric dysplasia and EGC at an early stage. We previously reported that gastric washes closely mirrored biopsy results in DNA methylation level [6]. We also found an approximately good correlation of DNA methylation levels from FFPE and gastric washes (Fig. 3b). In our present clinical study, Sox17 showed significantly different methylation levels between pre- and post-treatment in EGC patients using gastric washes ($p<0.0001$) (Fig. 2). The dot plots results of Sox17 show significant differences in methylation levels between not only pre- and post-ER ($p<0.0001$) but also between pre-ER and gastritis samples. Additionally, there is a significant difference in methylation levels between gastritis with and without *H. pylori* infection (Supplementary Fig. 1a). Moreover, we could successfully identify the incomplete ER case based on the Sox17 methylation status in gastric washes (without decreasing Sox17 methylation levels), and additional resection resulted in the successful removal of residual cancer (Supplementary Fig. 1b, c). However, without follow-up studies, it is still uncertain how methylation levels affect precancerous regions (which have not been viewed endoscopically) remaining in the stomach after ER. Moreover, it may be more useful to detect EGC with high sensitivity by a combination of markers including those we previously reported [6].

In summary, we have shown that Sox17 expression is often epigenetically silenced in gastric cancer. Such silencing of Sox17 was mediated by DNA methylation and the introduction of Sox17 into cancer cells suppressed cell growth. Understanding the precise role played by Sox17 in gene transcription will not only increase our understanding of the biology of gastric cancer but it may also enable epigenetic silencing of Sox17 to serve as a useful molecular target for diagnosis. These data raise hope for the possibility of obtaining gastric washes without requiring an endoscope in EGC detection, an approach that should be tested in future trials.

Acknowledgments This work was supported in part by The Japanese Foundation for Research and Promotion of Endoscopy (JFE) and The Japanese Society of Gastroenterology (JSGE). Yoshiyuki Watanabe is a member of The Japan Gastroenterological Endoscopy Society (JGES) and the JSGE and is supported by a generous gift from both the JFE and the JSGE. The authors are grateful to Ms. Tina Butterfield for her critical advice.

Conflicts of interest None.

References

1. Hohenberger P, Gretschel S. Gastric cancer. Lancet. 2003;362:305–15.
2. Jemal A, Siegel R, Xu J, Ward E. Cancer statistics, 2010. CA Cancer J Clin. 2010;60:277–300.
3. Parkin DM. Global cancer statistics in the year 2000. Lancet Oncol. 2001;2:533–43.
4. Denk H, Tappeiner G, Davidovits A, Holzner HJ. The carcinoembryonic antigen (CEA) in carcinomata of the stomach. Virchows Arch A Pathol Pathol Anat. 1973;360:339–47.
5. Koprowski H, Steplewski Z, Mitchell K, Herlyn M, Herlyn D, Fuhrer P. Colorectal carcinoma antigens detected by hybridoma antibodies. Somatic Cell Genet. 1979;5:957–71.
6. Watanabe Y, Kim HS, Castoro RJ, Chung W, Estecio MR, Kondo K, Guo Y, Ahmed SS, Toyota M, Itoh F, Suk KT, Cho MY, Shen L, Jelinek J, Issa JP. Sensitive and specific detection of early gastric cancer with DNA methylation analysis of gastric washes. Gastroenterology. 2009;136:2149–58.
7. Feltus FA, Lee EK, Costello JF, Plass C, Vertino PM. Predicting aberrant CpG island methylation. Proc Natl Acad Sci U S A. 2003;100:12253–8.
8. Ushijima T, Sasako M. Focus on gastric cancer. Cancer Cell. 2004;5:121–5.
9. Horii A, Nakatsuru S, Miyoshi Y, Ichii S, Nagase H, Kato Y, Yanagisawa A, Nakamura Y. The APC gene, responsible for familial adenomatous polyposis, is mutated in human gastric cancer. Cancer Res. 1992;52:3231–3.
10. Nanus DM, Kelsen DP, Mentle IR, Altorki N, Albino AP. Infrequent point mutations of ras oncogenes in gastric cancers. Gastroenterology. 1990;98:955–60.
11. Maesawa C, Tamura G, Suzuki Y, Ogasawara S, Sakata K, Kashiwaba M, Satodate R. The sequential accumulation of genetic alterations characteristic of the colorectal adenoma-carcinoma sequence does not occur between gastric adenoma and adenocarcinoma. J Pathol. 1995;176:249–58.
12. Laird PW. The power and the promise of DNA methylation markers. Nat Rev Cancer. 2003;3:253–66.
13. Issa JP. CpG island methylator phenotype in cancer. Nat Rev Cancer. 2004;4:988–93.
14. Ushijima T. Detection and interpretation of altered methylation patterns in cancer cells. Nat Rev Cancer. 2005;5:223–31.
15. Belinsky SA, Klinge DM, Dekker JD, Smith MW, Bocklage TJ, Gilliland FD, Crowell RE, Karp DD, Stidley CA, Picchi MA. Gene promoter methylation in plasma and sputum increases with lung cancer risk. Clin Cancer Res. 2005;11:6505–11.
16. Itzkowitz SH, Jandorf L, Brand R, Rabeneck L, Schroy III PC, Sontag S, Johnson D, Skoletsky J, Durkee K, Markowitz S, Shuber A. Improved fecal DNA test for colorectal cancer screening. Clin Gastroenterol Hepatol. 2007;5:111–7.
17. Suzuki H, Toyota M, Sato H, Sonoda T, Sakauchi F, Mori M. Roles and causes of abnormal DNA methylation in gastrointestinal cancers. Asian Pac J Cancer Prev. 2006;7:177–85.
18. Kusano M, Toyota M, Suzuki H, Akino K, Aoki F, Fujita M, Hosokawa M, Shinomura Y, Imai K, Tokino T. Genetic, epigenetic, and clinicopathologic features of gastric carcinomas with the CpG island methylator phenotype and an association with Epstein–Barr virus. Cancer. 2006;106:1467–79.
19. Issa JP, Shen L, Toyota M. CIMP, at last. Gastroenterology. 2005;129:1121–4.
20. Toyota M, Ohe-Toyota M, Ahuja N, Issa JP. Distinct genetic profiles in colorectal tumors with or without the CpG island methylator phenotype. Proc Natl Acad Sci U S A. 2000;97:710–5.
21. Toyota M, Ahuja N, Suzuki H, Itoh F, Ohe-Toyota M, Imai K, Baylin SB, Issa JP. Aberrant methylation in gastric cancer associated with the CpG island methylator phenotype. Cancer Res. 1999;59:5438–42.
22. Toyota M, Ahuja N, Ohe-Toyota M, Herman JG, Baylin SB, Issa JP. CpG island methylator phenotype in colorectal cancer. Proc Natl Acad Sci U S A. 1999;96:8681–6.
23. Shen L, Kondo Y, Rosner GL, Xiao L, Hernandez NS, Vilaythong J, Houlihan PS, Krouse RS, Prasad AR, Einspahr JG, Buckmeier J, Alberts DS, Hamilton SR, Issa JP. MGMT promoter methylation and field defect in sporadic colorectal cancer. J Natl Cancer Inst. 2005;97:1330–8.
24. Dakubo GD, Jakupciak JP, Birch-Machin MA, Parr RL. Clinical implications and utility of field cancerization. Cancer Cell Int. 2007;7:2.
25. Kim SK, Jang HR, Kim JH, Noh SM, Song KS, Kim MR, Kim SY, Yeom YI, Kim NS, Yoo HS, Kim YS. The epigenetic silencing of LIMS2 in gastric cancer and its inhibitory effect on cell migration. Biochem Biophys Res Commun. 2006;349:1032–40.
26. Shen L, Kondo Y, Guo Y, Zhang J, Zhang L, Ahmed S, Shu J, Chen X, Waterland RA, Issa JP. Genome-wide profiling of DNA methylation reveals a class of normally methylated CpG island promoters. PLoS Genet. 2007;3:2023–36.
27. Estecio MR, Yan PS, Huang TH, Issa JP. Methylated CpG island amplification and microarray (MCAM) for high-throughput analysis of DNA methylation. CSH Protoc 2008;2008:db.
28. Estecio MR, Yan PS, Ibrahim AE, Tellez CS, Shen L, Huang TH, Issa JP. High-throughput methylation profiling by MCA coupled to CpG island microarray. Genome Res. 2007;17:1529–36.
29. Kroeger H, Jelinek J, Estecio MR, He R, Kondo K, Chung W, Zhang L, Shen L, Kantarjian HM, Bueso-Ramos CE, Issa JP. Aberrant CpG island methylation in acute myeloid leukemia is accentuated at relapse. Blood. 2008;112:1366–73.
30. Okamoto Y, Sawaki A, Ito S, Nishida T, Takahashi T, Toyota M, Suzuki H, Shinomura Y, Takeuchi I, Shinjo K, An B, Ito H, Yamao K, Fujii M, Murakami H, Osada H, Kataoka H, Joh T, Sekido Y, Kondo Y. Aberrant DNA methylation associated with aggressiveness of gastrointestinal stromal tumour. Gut 2011; doi:10.1136/gut.2011.241034.
31. Akino K, Toyota M, Suzuki H, Imai T, Maruyama R, Kusano M, Nishikawa N, Watanabe Y, Sasaki Y, Abe T, Yamamoto E, Tarasawa I, Sonoda T, Mori M, Imai K, Shinomura Y, Tokino T. Identification of DFNA5 as a target of epigenetic inactivation in gastric cancer. Cancer Sci. 2007;98:88–95.
32. Kikuchi T, Itoh F, Toyota M, Suzuki H, Yamamoto H, Fujita M, Hosokawa M, Imai K. Aberrant methylation and histone deacetylation of cyclooxygenase 2 in gastric cancer. Int J Cancer. 2002;97:272–7.
33. Maruyama R, Akino K, Toyota M, Suzuki H, Imai T, Ohe-Toyota M, Yamamoto E, Nojima M, Fujikane T, Sasaki Y, Yamashita T, Watanabe Y, Hiratsuka H, Hirata K, Itoh F, Imai K, Shinomura Y, Tokino T. Cytoplasmic RASSF2A is a proapoptotic mediator whose expression is epigenetically silenced in gastric cancer. Carcinogenesis. 2008;29:1312–8.
34. Murai M, Toyota M, Suzuki H, Satoh A, Sasaki Y, Akino K, Ueno M, Takahashi F, Kusano M, Mita H, Yanagihara K, Endo T, Hinoda Y, Tokino T, Imai K. Aberrant methylation and silencing

of the BNIP3 gene in colorectal and gastric cancer. Clin Cancer Res. 2005;11:1021–7.
35. Nojima M, Suzuki H, Toyota M, Watanabe Y, Maruyama R, Sasaki S, Sasaki Y, Mita H, Nishikawa N, Yamaguchi K, Hirata K, Itoh F, Tokino T, Mori M, Imai K, Shinomura Y. Frequent epigenetic inactivation of SFRP genes and constitutive activation of Wnt signaling in gastric cancer. Oncogene. 2007;26:4699–713.
36. Obata T, Toyota M, Satoh A, Sasaki Y, Ogi K, Akino K, Suzuki H, Murai M, Kikuchi T, Mita H, Itoh F, Issa JP, Tokino T, Imai K. Identification of HRK as a target of epigenetic inactivation in colorectal and gastric cancer. Clin Cancer Res. 2003;9:6410–8.
37. Satoh A, Toyota M, Itoh F, Sasaki Y, Suzuki H, Ogi K, Kikuchi T, Mita H, Yamashita T, Kojima T, Kusano M, Fujita M, Hosokawa M, Endo T, Tokino T, Imai K. Epigenetic inactivation of CHFR and sensitivity to microtubule inhibitors in gastric cancer. Cancer Res. 2003;63:8606–13.
38. Ueno M, Toyota M, Akino K, Suzuki H, Kusano M, Satoh A, Mita H, Sasaki Y, Nojima M, Yanagihara K, Hinoda Y, Tokino T, Imai K. Aberrant methylation and histone deacetylation associated with silencing of SLC5A8 in gastric cancer. Tumour Biol. 2004;25:134–40.
39. Watanabe Y, Toyota M, Kondo Y, Suzuki H, Imai T, Ohe-Toyota M, Maruyama R, Nojima M, Sasaki Y, Sekido Y, Hiratsuka H, Shinomura Y, Imai K, Itoh F, Tokino T. PRDM5 identified as a target of epigenetic silencing in colorectal and gastric cancer. Clin Cancer Res. 2007;13:4786–94.
40. Watanabe Y, Kato N, Maehata T, Okamoto M, Tsuda T, Hattori S, Yamauchi S, Fujita K, Baba S, Nakaya S, Inaba H, Kitajima S, Suzuki M, Niwa H, Itoh F. Safer endoscopic gastric mucosal resection: preoperative proton pump inhibitor administration. J Gastroenterol Hepatol. 2006;21:1675–80.
41. Ono H, Hasuike N, Inui T, Takizawa K, Ikehara H, Yamaguchi Y, Otake Y, Matsubayashi H. Usefulness of a novel electrosurgical knife, the insulation-tipped diathermic knife-2, for endoscopic submucosal dissection of early gastric cancer. Gastric Cancer. 2008;11:47–52.
42. Toyota M, Ho C, Ahuja N, Jair KW, Li Q, Ohe-Toyota M, Baylin SB, Issa JP. Identification of differentially methylated sequences in colorectal cancer by methylated CpG island amplification. Cancer Res. 1999;59:2307–12.
43. Sano T. Evaluation of the gastric cancer treatment guidelines of the Japanese Gastric Cancer Association. Gan To Kagaku Ryoho. 2010;37:582–6.
44. Du YC, Oshima H, Oguma K, Kitamura T, Itadani H, Fujimura T, Piao YS, Yoshimoto T, Minamoto T, Kotani H, Taketo MM, Oshima M. Induction and down-regulation of Sox17 and its possible roles during the course of gastrointestinal tumorigenesis. Gastroenterology. 2009;137:1346–57.
45. Toyota M, Issa JP. The role of DNA hypermethylation in human neoplasia. Electrophoresis. 2000;21:329–33.
46. Toyota M, Issa JP. CpG island methylator phenotypes in aging and cancer. Semin Cancer Biol. 1999;9:349–57.
47. Issa JP, Ahuja N, Toyota M, Bronner MP, Brentnall TA. Accelerated age-related CpG island methylation in ulcerative colitis. Cancer Res. 2001;61:3573–7.
48. Zhang W, Glockner SC, Guo M, Machida EO, Wang DH, Easwaran H, Van NL, Herman JG, Schuebel KE, Watkins DN, Ahuja N, Baylin SB. Epigenetic inactivation of the canonical Wnt antagonist SRY-box containing gene 17 in colorectal cancer. Cancer Res. 2008;68:2764–72.

THE JOURNAL OF BIOLOGICAL CHEMISTRY VOL. 287, NO. 16, pp. 12975–12984, April 13, 2012

CHFR Protein Regulates Mitotic Checkpoint by Targeting PARP-1 Protein for Ubiquitination and Degradation*[S]

Received for publication, November 9, 2011, and in revised form, February 13, 2012 Published, JBC Papers in Press, February 15, 2012, DOI 10.1074/jbc.M111.321828

Lisa Kashima[‡§], Masashi Idogawa[‡], Hiroaki Mita[‡], Miki Shitashige[¶], Tesshi Yamada[¶], Kazuhiro Ogi[‡], Hiromu Suzuki[‡‖], Minoru Toyota[‖], Hiroyoshi Ariga[§], Yasushi Sasaki[‡], and Takashi Tokino[‡1]

From the [‡]Department of Medical Genome Sciences, Research Institute for Frontier Medicine, Sapporo Medical University, Sapporo 060-8556, Japan, the [¶]Chemotherapy Division and Cancer Proteomics Project, National Cancer Research Institute, Tokyo 104-0045, Japan, the [‖]Department of Molecular Biology, Sapporo Medical University, Sapporo 060-8556, Japan, and the [§]Graduate School of Pharmaceutical Sciences, Hokkaido University, Sapporo 060-0812, Japan

Background: CHFR is a tumor suppressor that arrests the cell cycle at prophase.
Results: CHFR regulates the mitotic checkpoint via PARP-1 ubiquitination and degradation.
Conclusion: The interaction between CHFR and PARP-1 plays an important role in cell cycle regulation and cancer therapy.
Significance: Our data shed new light on a potential strategy for the combined usage of PARP inhibitors with microtubule inhibitors.

The mitotic checkpoint gene *CHFR* (checkpoint with forkhead-associated (FHA) and RING finger domains) is silenced by promoter hypermethylation or mutated in various human cancers, suggesting that CHFR is an important tumor suppressor. Recent studies have reported that CHFR functions as an E3 ubiquitin ligase, resulting in the degradation of target proteins. To better understand how CHFR suppresses cell cycle progression and tumorigenesis, we sought to identify CHFR-interacting proteins using affinity purification combined with mass spectrometry. Here we show poly(ADP-ribose) polymerase 1 (PARP-1) to be a novel CHFR-interacting protein. In *CHFR*-expressing cells, mitotic stress induced the autoPARylation of PARP-1, resulting in an enhanced interaction between CHFR and PARP-1 and an increase in the polyubiquitination/degradation of PARP-1. The decrease in PARP-1 protein levels promoted cell cycle arrest at prophase, supporting that the cells expressing *CHFR* were resistant to microtubule inhibitors. In contrast, in *CHFR*-silenced cells, polyubiquitination was not induced in response to mitotic stress. Thus, PARP-1 protein levels did not decrease, and cells progressed into mitosis under mitotic stress, suggesting that *CHFR*-silenced cancer cells were sensitized to microtubule inhibitors. Furthermore, we found that cells from *Chfr* knockout mice and *CHFR*-silenced primary gastric cancer tissues expressed higher levels of PARP-1 protein, strongly supporting our data that the interaction between CHFR and PARP-1 plays an important role in cell cycle regulation and cancer therapeutic strategies. On the basis of our studies, we demonstrate a significant advantage for use of combinational chemotherapy with PARP inhibitors for cancer cells resistant to microtubule inhibitors.

The checkpoint with forkhead-associated (FHA)[2] and RING finger domains (*CHFR*) gene is frequently inactivated by promoter hypermethylation in various human malignancies. *Chfr*-deficient mice are cancer-prone (1), suggesting that the CHFR protein functions as a tumor suppressor (2, 3). CHFR is a nuclear protein and plays an important role in the early mitotic checkpoint by actively delaying passage into mitosis in response to mitotic stress caused by microtubule inhibitors (4). However, it is not fully understood how CHFR acts in the mitotic checkpoint or how it is regulated in response to mitotic stress. CHFR contains an N-terminal FHA domain, a central RING finger domain, and a C-terminal cysteine-rich (CR) region. The FHA domain is required for the mitotic checkpoint (4). Additionally, we have reported previously that the FHA domain is required for the inhibition of NF-κB signaling (5). The RING finger domain of CHFR mediates its function as an E3 ubiquitin (Ub) ligase, and CHFR catalyzes the synthesis of lysine 48 (Lys-48)-linked and lysine 63 (Lys-63)-linked polyubiquitination chains, which promote target protein degradation and alter protein function, respectively (6–8). Recently, a novel poly(ADP-ribose)-binding zinc finger (PBZ) motif was identified in the CR region of CHFR (9).

Poly(ADP-ribosyl)ation (PARylation) is a posttranscriptional modification whereby poly(ADP-ribose) polymerases (PARPs) polymerize poly(ADP-ribose) onto acceptor proteins using NAD^+ as a substrate. PARP-1, the most abundant and founding member of the PARP family, is activated by a DNA strand break, PARylates acceptor proteins, and automodifies

* This research was supported in part by grants-in-aid for scientific research from the Ministry of Education, Culture, Sports, Science, and Technology of Japan (to T. T.) and the Kanzawa Medical Research Foundation (to L. K.).
[S] This article contains supplemental Figs. S1–S6, Table S1, methods, and references.
[1] To whom correspondence should be addressed: Department of Medical Genome Sciences, Research Institute for Frontier Medicine, Sapporo Medical University, S-1, W-17, Chuo-ku, Sapporo, 060-8556, Japan. Tel.: 81-11-611-2111 ext. 2410; Fax: 81-11-618-3313; E-mail: tokino@sapmed.ac.jp.

[2] The abbreviations used are: FHA, forkhead-associated; CR, cysteine-rich; Ub, ubiquitin; PBZ, poly(ADP-ribose)-binding; PARylation, poly(ADP-ribosyl)ation; MEF, mouse embryonic fibroblasts; ES, embryonic stem; DBD, DNA binding domain; AD, automodification domain; CD, catalytic domain; MI, mitotic index; DMSO, dimethyl sulfoxide.

PARP-1 itself. PARP-1 also initiates multiple cellular responses, including DNA repair, cell cycle checkpoint control, apoptosis, and transcription in the nucleus (10). In human cancers, the overexpression of PARP-1 has been reported in various human malignancies (11–15), indicating that deregulation of PARP-1 expression correlates with tumor development. Additionally, recent studies have suggested that PARP inhibitors could be used as anticancer drugs (16). However, the molecular mechanisms through which the deregulation of PARP-1 occurs or contributes to tumor development remain unclear. Furthermore, how PARP inhibitors exert their beneficial effects in tumor cells has not been established.

In this study, we identified PARP-1 as a novel CHFR binding protein and found a functional interaction that regulates the early mitotic checkpoint and tumorigenesis.

EXPERIMENTAL PROCEDURES

Cell Culture and Transfections—Human breast cancer cells (SK-BR-3 and ZR-75–1), human cervical carcinoma cells (HeLa), human colorectal cancer cells (HCT116 and DLD-1), human stomach cancer cells (HSC-44, MKN7, and MKN45), human oral squamous cells (HSC-3), human non-small cell lung cancer cells (LU99), and human embryonic kidney cells (HEK-293) used in this study were purchased from the ATCC or the Japan Collection of Research Bioresources. DLD-1 Tet-Off cells were double-transfected with regulatory pTet-Off (Clontech,) and responsive pTRE2-FLAG-CHFR or pTRE-pur control plasmids. HCT116 cells were transfected with iLenti-GFP PARP1 siRNAs or iLenti-GFP control plasmids (ABM). Colonies of cells stably transfected with iLenti-GFP PARP1 siRNA and iLenti-GFP were selected with G418, screened by immunoblotting, and named HCT116 siPARP1 and HCT116 siControl cells, respectively. All transfections were performed using Lipofectamine 2000 (Invitrogen).

Generation of Chfr Knockout Mice and MEFs—The *Chfr* knockout mice were generated as a standard knockout project (project ID no. OYC056) by Lexicon Pharmaceuticals, Inc. (supplemental Fig. S1 and methods). Briefly, the targeting vector was electroporated into Lex-1 ES cells derived from the 129SvEvBrd strain, and screened ES cell clones were injected into C57BL/6 blastocysts. Chimeric mice were backcrossed with C57BL/6 females or males at least seven times. Mice were maintained under specific pathogen-free conditions. The $Chfr^{+/-}$ mice were mated, and littermate primary MEFs were isolated from E14.5 mouse embryos and cultured in Dulbecco's modified Eagle's medium containing 10% fetal bovine serum.

Plasmids, siRNAs and Recombinant Adenoviruses—The expression plasmid vectors for cDNAs encoding full-length CHFR and deletion constructs, and the corresponding adenoviruses have been reported previously (5). The CHFR ΔE3 mutant, lacking amino acids 292 to 309, and the ΔPBZ mutant, lacking amino acids 619 to 644, were inserted into a FLAG-tagged pCMV-tag2B vector (Stratagene). The expression vectors for cDNAs encoding full-length PARP-1 and deletion constructs have been reported previously (17). The pCI-neo-2S-ubiquitin plasmid expressing human ubiquitin was kindly provided by Dr. Hideyoshi Yokosawa of Hokkaido University, Japan. iLenti-GFP siRNA and iLenti-GFP PARP1 siRNA, which contain the oligonucleotide 5′-GTGAAGAA-GCTGACAGTAAATCCTGGCAC-3′, were designed and purchased from ABM. The siRNAs targeting human *PARP1* (5′-GAAAACAGGUAUUGGAUAU-3′, 5′-GUGUCAAAG-GUUUGGGCAA-3′ and 5′-CAUGGGAGCUCUUGAAAU-A-3′), *AURKA* (5′-UGUCAUUCGAAGAGAGUUATT-3′, 5′-CCAUAUAACCUGACAGGAATT-3′, and 5′-AGUCA-UAGCAUGUGUGUAATT) and the control siRNAs were purchased from B-Bridge. The siRNA targeting human *PLK1* (5′-rGUrCUrCrArArGrGrCrCUrCrCUrArAUrATT-3′) was purchased from Sigma (RNA nucleotides were indicated as "rN").

Antibodies—The antibodies used for experiments were as follows: anti-FLAG antibody (M2, Sigma), anti-CHFR antibodies (PAB6325 and 1H3-A12, Abnova; 12169-1-AP, Proteintech), anti-PARP-1 antibodies (C2–10, BD Biosciences; catalog no. 611038, BD Biosciences; H-250, Santa Cruz Biotechnology; catalog no. 9542, Cell Signaling Technology; ALX-210–619, Enzo Life Science), anti-ubiquitin antibody (P4D1, Santa Cruz Biotechnology), anti-PAR antibodies (10H, Tulip BioLabs; catalog no. 4336-APC-050, Trevigen), anti-Plk-1 antibody (catalog no. 33–1700, Zymed Laboratories Inc.), anti-GFP antibody (sc-8334, Santa Cruz Biotechnology), anti-actin antibody (MAB1501R, Millipore) and HRP-conjugated secondary antibodies (Santa Cruz Biotechnology).

Co-immunoprecipitation Assays—Co-immunoprecipitation assays were performed as previously described (5). In brief, cells were washed with PBS and lysed in HBST buffer (10 mM HEPES, pH 7.4; 150 mM NaCl, 0.5% Triton X-100, 10 μM MG132 and protease inhibitor mixture). For endogenous binding analysis, the nuclear extracts were isolated and diluted 5-fold with HBST. The lysates were co-immunoprecipitated with antibodies.

Protein Identification by Mass Spectrometry—The analysis of proteins by LC-MS/MS was performed as previously reported (14).

In Vitro Protein-Protein Binding Assays—Full-length or deletion mutants of biotinylated PARP-1 were generated by *in vitro* translation as previously reported (17). HEK-293T cells were mock transfected or transfected with Flag-CHFR expression vectors, and the Flag-CHFR protein was purified using an anti-Flag M2 antibody. The immunoprecipitants were incubated with *in vitro* translated PARP-1 proteins at 4 °C overnight in HBST buffer. The complexes were washed three times with HBST buffer, eluted by incubation for 1 h at 4 °C with 150 ng/μl of 3x Flag peptide (SIGMA) and subjected to SDS-PAGE followed by immunoblotting.

In Vitro Ubiquitination Assays—HEK-293T cells were mock-transfected or transfected with Myc-CHFR expression vectors. The cells were lysed in lysis buffer (50 mM Tris-HCl (pH 7.4), 150 mM NaCl, 1% Triton X-100, 1 mM NaV, 10 mM NaF, 1 mM DTT, and protease inhibitor mixture). The Myc-CHFR and PARP-1 complexes were immunoprecipitated with anti-Myc resins. The resin was washed three times with lysis buffer and incubated with 0.03 μg/μl of FLAG-Ub, 8.3 ng/μl of E1 and 500 nM E2 (UbcH5c or Ube2N) in the reaction mixture (50 mM Tris-HCL (pH 7.4) 5 mM $MgCl_2$, 2 mM DTT and 5 mM ATP) for 30 min at 37 °C. The supernatants from the reactions were collected and analyzed by immunoblotting.

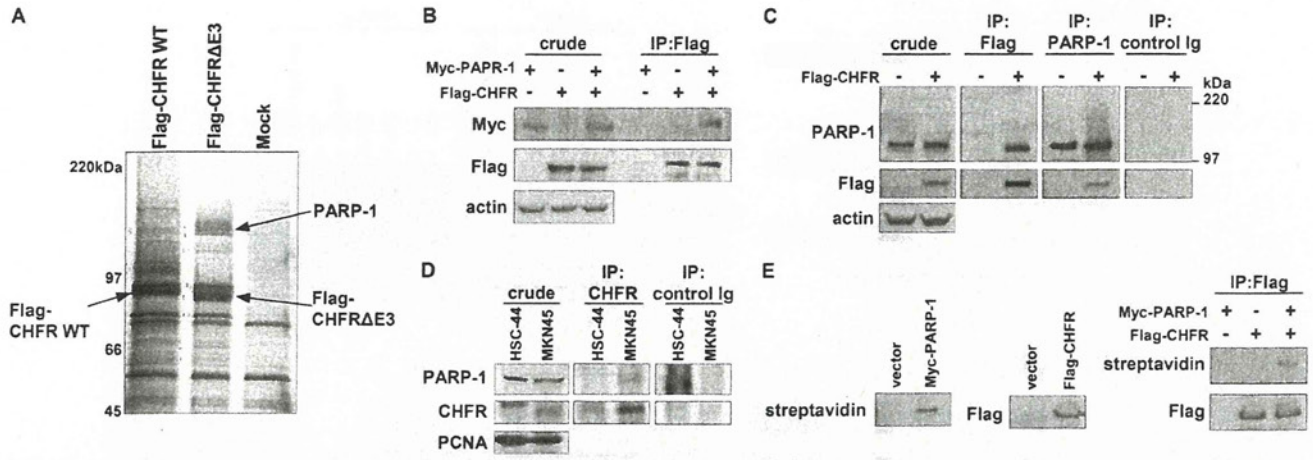

FIGURE 1. **CHFR interacts with PARP-1.** *A*, HEK-293T cells were transiently transfected with FLAG-CHFR WT or FLAG-CHFR-deleted E3 activity (ΔE3) expression vectors or mock-transfected, and cell lysates were immunoprecipitated with anti-FLAG resin. Proteins that coimmunoprecipitated with FLAG-CHFR were separated by SDS-PAGE and negative gel staining and subjected to LC-MS/MS analysis. PARP-1 was identified as a CHFR-interacting protein. *B*, HCT116 cells, which do not express endogenous CHFR, were transfected with FLAG-CHFR and Myc-PARP-1 expression vectors. The cell lysates were immunoprecipitated (*IP*) with an anti-FLAG antibody, and Myc-PARP-1 was coimmunoprecipitated. Immunoblotting was performed with antibodies against each of the indicated proteins. *C*, HeLa cells, which do not express endogenous CHFR, were transfected with FLAG-CHFR expression vectors. The cell lysates were immunoprecipitated using anti-FLAG or anti-PARP-1 antibodies or control Ig. Immunoblotting was performed with antibodies against the indicated proteins. Endogenous PARP-1 and FLAG-CHFR were coimmunoprecipitated with FLAG-CHFR and PARP-1, respectively. *D*, the nuclear extracts form MKN45 and HSC-44cells, which express or do not express endogenous CHFR, respectively, were immunoprecipitated using anti-CHFR antibodies or control Ig. Immunoblotting was performed with antibodies against the indicated proteins. *E*, FLAG-CHFR was purified from HEK-293T cells with an anti-FLAG antibody and incubated with the biotinylated PARP-1 generated by *in vitro* translation. The complexes were thoroughly washed and analyzed by blotting with an anti-FLAG antibody or streptavidin-HRP.

RT-PCR—For RT-PCR analysis, cDNAs were synthesized from 5 μg of total mouse RNA with SuperScript III (Invitrogen). The PCR conditions included an initial denaturation step at 94 °C for 2 min, followed by 28 cycles (for *Parp1*), 27 cycles (for *Chfr*) or 21 cycles (for *Gapdh*) at 94 °C for 30 s, 63 °C (for *Parp1*), 61 °C (for *Chfr*) or 55 °C (for *Gapdh*) for 30 s, and 72 °C for 1 min. Oligonucleotide primer sequences were as follows: *Parp1* sense (5′-GACAGCGTGCAGGCCAAGGT-3′) and antisense (5′-CACAGGCGCTTCAGGTGGGG-3′), *Chfr* sense (5′-ATGGAGCTACACGGGGAAGAGCA-3′) and antisense (5′-TTGGCAGGCTCCAATTCCTCATGGT-3′), and *Gapdh* sense (5′-CAACTCACTCAAGATTGTCAGCAA-3′) and antisense (5′-TACTTGGCAGGTTTCTCCAGGC-3′). PCR products were visualized by electrophoresis on 1.5% agarose gels.

Tissue Samples and Immunohistochemistry—To study PARP-1 expression in primary gastric cancers, 19 paraffin-embedded samples from Japanese patients were selected randomly. Informed consent was obtained from all patients before the samples were collected. The samples were stained with an anti PARP-1 antibody (catalog no. 9542, Cell Signaling Technology) using the avidin-biotin complex method as described previously (17). The staining was scored using a three-tiered scoring system (+, weak; ++, moderate; +++, strong).

DNA Methylation Analysis—Genomic DNA from paraffin-embedded gastric cancer samples was purified using the QIAamp DNA FFPE tissue kit (Qiagen) following bisulfite treatment using the EpiTect bisulfite kit (Qiagen). To analyze the percent methylation of *CHFR*, MetyLight assays were performed using primers and probes as reported previously (18, 19). Alu was used for normalization of data, and genomic DNA from HCT116 cells in which *CHFR* is 100% methylated was used as a reference. Primers, probes, and the percentage of methylated reference were determined as described previously (20). We used a percentage of methylated reference cutoff of 4 to distinguish methylation-positive (percentage of methylated reference > 4) from methylation-negative (percentage of methylated reference ≤ 4) samples.

Mitotic Index—Cells (5×10^5 or 1×10^6) were cultured for 24 h in 6-well plates and transfected with plasmids or siRNAs. Twenty-four hours after transfection, cells were treated with 1 μM docetaxel or 3 mM 3-am inobenzamide (3AB) for an additional 16 h. Thereafter, the cells were harvested with trypsin, and the percentages of mitotic cells were counted as reported previously (21).

Flow Cytometry—One million cells were cultured in 6-mm plates and treated with 1 μM docetaxel or 10 mM 3AB for 48 h and subjected to flow cytometry as reported previously (21). The data were analyzed using FlowJo software.

RESULTS

CHFR Interacts with PARP-1—To better understand how CHFR suppresses cell cycle progression and tumorigenesis and how it is functionally regulated in response to mitotic stress, we identified CHFR-interacting proteins using affinity purification by liquid chromatography combined with tandem mass spectrometry (LC-MS/MS). As CHFR has Ub ligase activity, we used a CHFR mutant lacking the 18 amino acids (292 to 309) that form the core amino acid sequence for E3 Ub ligase activity (FLAG-CHFR ΔE3). We then compared the proteins that coimmunoprecipitated with FLAG-CHFR to those that coimmunoprecipitated with FLAG-CHFR ΔE3. On the basis of these analyses, we identified PARP-1 as a candidate CHFR-interacting protein that bound to CHFR ΔE3 more strongly than to WT

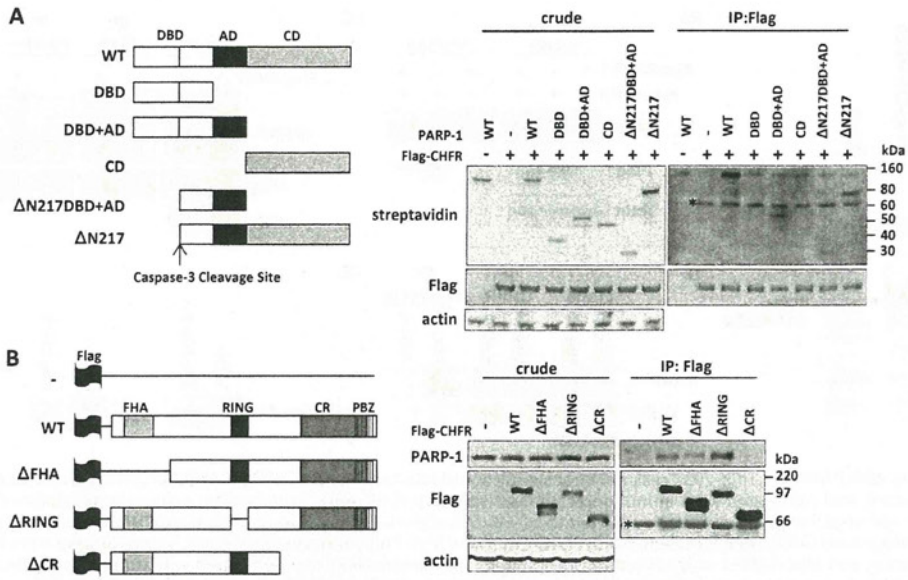

FIGURE 2. **Identification of the regions required for the interaction between CHFR and PARP-1.** *A*, PARP-1 deletion mutants used in this study (*left panel*). FLAG-CHFR was purified from HEK-293T cells with an anti-FLAG antibody and incubated with the biotinylated PARP-1 deletion mutants generated by *in vitro* translation. The crude samples and the complexes were analyzed by blotting with anti-FLAG or anti-actin antibodies or streptavidin-HRP (*right panel*). *ΔN217*, Δ N terminus 217 residues; *IP*, immunoprecipitation. *B*, CHFR deletion mutants used in this study (*left panel*). HCT116 cells were transfected with FLAG-CHFR deletion constructs. The cell lysates were immunoprecipitated with an anti-FLAG antibody, and endogenous PARP-1 was coimmunoprecipitated (*right panel*). Immunoblotting was performed with antibodies against each of the indicated proteins. *ΔFHA*, Δ FHA domain; *ΔRING*, Δ RING finger domain; *ΔCR*, Δ CR domain; *, nonspecific bands.

CHFR (Fig. 1*A*). An interaction between FLAG-CHFR and Myc-PARP-1 was validated in HCT116 cells (Fig. 1*B*). Furthermore, an interaction between endogenous PARP-1 and FLAG-CHFR was confirmed in FLAG-CHFR transfected HeLa cells (Fig. 1*C*). To confirm an endogenous binding between CHFR and PARP-1, coimmunoprecipitation assays were performed in MKN45 and HSC-44 cells that express or do not express CHFR, respectively (Fig. 1*D*). The interaction between CHFR and PARP-1 *in vitro* was also demonstrated (Fig. 1*E*). These data indicate that CHFR interacts with PARP-1.

Because PARP-1 contains three conserved domains, a DNA-binding domain (DBD), an automodification domain (AD), and a catalytic domain (CD), we investigated which domain of PARP-1 was essential for its interaction with CHFR. PARP-1 deletion mutants were translated *in vitro* and incubated with FLAG-CHFR. The PARP-1 CD mutant lacking both the DBD and the AD was not able to bind to FLAG-CHFR at all, whereas the PARP-1 DBD+AD mutant lacking the CD could bind to FLAG-CHFR (Fig. 2*A*). Moreover, the PARP-1 ΔN217 and ΔN217DBD+AD mutants retaining the AD were coimmunoprecipitated with FLAG-CHFR. These data suggest that the AD of PARP-1 is mainly required for its physiological interaction with CHFR.

We next mapped the domain of CHFR that is required for its interaction with PARP-1. Several FLAG-CHFR deletion mutants were expressed in HCT116 cells, and endogenous PARP-1 was coimmunoprecipitated with an anti-FLAG antibody. The CHFR ΔCR mutant was unable to interact with PARP-1, suggesting that CHFR interacts with PARP-1 via its CR region (Fig. 2*B*). The CHFR ΔRING mutant lacking the RING finger domain, which is responsible for Ub ligase activity, associated with PARP-1 more stably than with CHFR WT, consistent with the results shown in Fig. 1*A*.

CHFR Polyubiquitinates PARP-1 and Causes Cell Cycle Arrest via PARP-1 Degradation—As shown in Figs. 1*A* and 2*B*, the amount of PARP-1 that bound to CHFR mutants lacking Ub ligase activity was greater than the amount that bound to CHFR WT. In addition, immunoprecipitated PARP-1 exhibited a 100–200 kDa smear upon immunoblotting only when FLAG-CHFR was overexpressed in HeLa cells, which do not express endogenous CHFR (Fig. 1*C*). These data suggested that PARP-1 was polyubiquitinated by CHFR. Then, we performed *in vitro* ubiquitination assays. The complex of Myc-CHFR with endogenous PARP-1 was coimmunoprecipitated with an anti-Myc antibody and incubated with FLAG-Ub, E1, and E2 (UbcH5c or Ube2N) under standard ubiquitination assay conditions. Because CHFR was found to catalyze both Lys-48-linked and Lys-63-linked polyubiquitination, we examined both UbcH5c, which promotes the synthesis of polyUb chains of various linkages, including Lys-48 and Lys-63, and Ube2N (also known as Ubc13), which catalyzes the synthesis of specific Lys-63 polyUb chains (Fig. 3*A*). The polyubiquitination of PARP-1 was observed in a FLAG-CHFR-dependent manner in the presence of either UbcH5c or Ube2N (Fig. 3*A*). The polyubiquitination mediated by Ube2N was lower when compared with that mediated by UbcH5c, indicating that CHFR catalyzed not only Lys-63-linked but also Lys-48-linked and other polyubiquitinations of PARP-1.

To examine whether CHFR polyubiquitinated PARP-1 in cells, we transfected CHFR WT and CHFR ΔE3 into HCT116 cells, which do not express endogenous CHFR. Overexpression of CHFR WT promoted polyubiquitination of PARP-1, but overexpression of CHFR ΔE3 did not (Fig. 3*B*). Treatment with MG132, a proteasome inhibitor, increased the polyUb smear in both CHFR WT and ΔE3-transfected cells, suggesting that PARP-1 could be polyubiquitinated in part by several E3 ligases and degraded by the

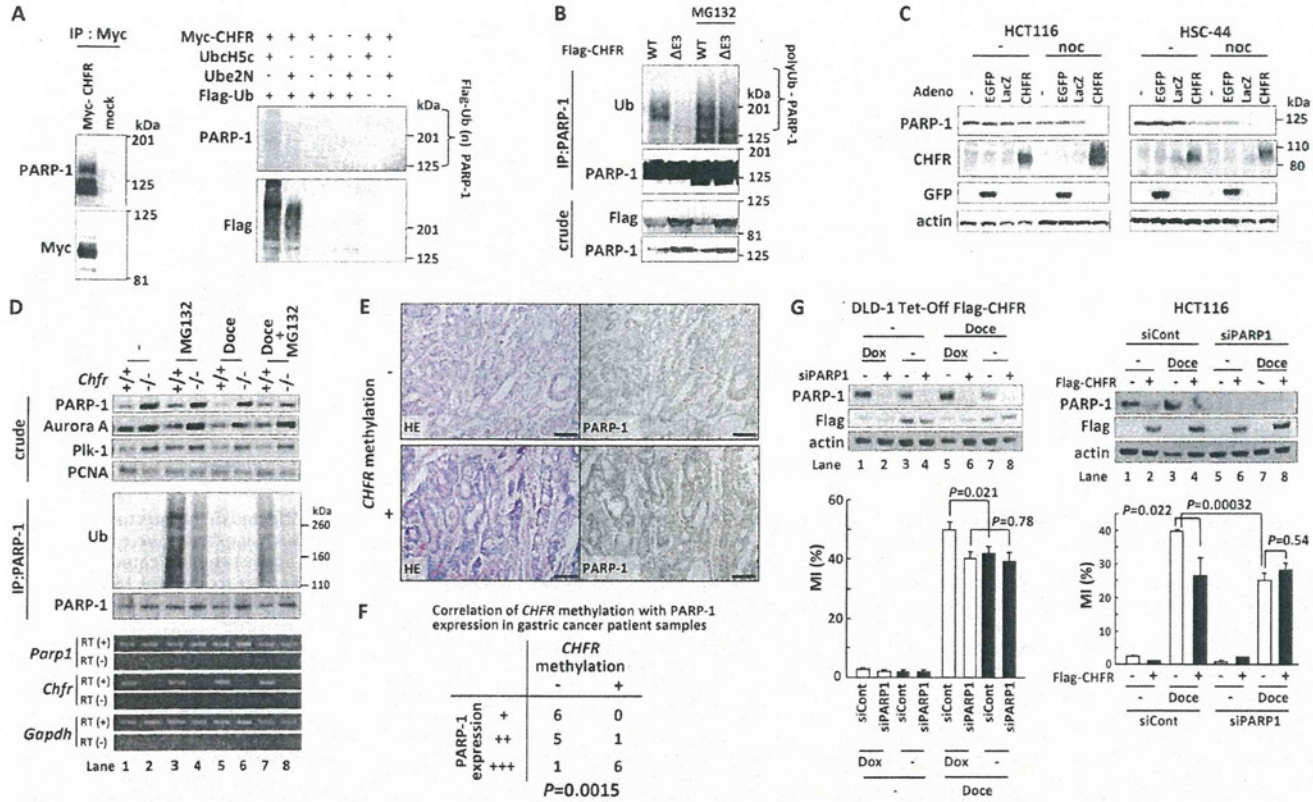

FIGURE 3. **CHFR polyubiquitinates PARP-1 and caused cell cycle arrest via PARP-1 degradation.** *A*, HEK-293T cells were mock-transfected or transfected with Myc-CHFR expression vectors, and PARP-1 and Myc-CHFR complexes were coimmunoprecipitated (*IP*) with an anti-Myc antibody (*left panel*). The resins were thoroughly washed, and *in vitro* ubiquitination assays were performed (*right panel*). Immunoblotting was performed with antibodies against each of the indicated proteins. *B*, HCT116 cells were transfected with FLAG-CHFR or FLAG-CHFR ΔE3 expression vectors. After transfection for 24 h, the cells were treated with or without 10 μM MG132 for 4 h. The cell lysates were immunoprecipitated with an anti-PARP-1 antibody, and the precipitates were examined by immunoblotting with anti-ubiquitin (*Ub*), anti-PARP-1, or anti-FLAG antibodies. *C*, HCT116 and HSC44 cells, which do not express endogenous CHFR, were infected with adenoviruses expressing CHFR (CHFR WT), enhanced green fluorescent protein (*EGFP*), or LacZ. After infection for 64 h, the cells were treated with 0.5 μg/ml of nocodazole (*noc*) or DMSO (-) for 27 h. The cell lysates were examined by immunoblotting with the indicated antibodies. *D*, $Chfr^{+/+}$ or $Chfr^{-/-}$ MEFs were treated with 1 μM docetaxel for 12 h, and 10 μM MG132 or DMSO was added following 4 h of incubation. Nuclear extractions were collected using the nuclear extract kit (Active Motif, Santa Clara, CA) and subjected to immunoprecipitation and immunoblotting with antibodies against each of the indicated proteins (*top panel*). RT-PCR was also performed (*bottom panel*). *E*, primary gastric cancer samples were stained using an anti-PARP-1 antibody. CHFR methylation status was analyzed as described under "Experimental Procedures." Magnification ×10. *Scale bar* = 100 μm. *F*, statistical analysis of CHFR methylation status and PARP-1 expression levels from 19 primary gastric cancer samples. The Wilcoxon rank test was used to determine whether there was an association between the CHFR methylation status and PARP-1 expression. The *p* value is indicated. *G*, DLD-1 Tet-Off cells inducibly expressing FLAG-CHFR (*DLD-1 Tet-Off FLAG-CHFR*) were cultured with or without 0.1 μg/ml of doxycycline (*Dox*) for 24 h and transfected with a mixture of three siRNAs targeting PARP-1 (*siPARP1*) or control oligonucleotides (*siCont*). After transfection for 4 h, the cells were cultured with or without 0.1 μg/ml of doxycycline for 22 h following treatment with 0.5 μM docetaxel (*Doce*) for 16 h, and the MI was determined (*left panel, bottom*). HCT116 cells with stably knocked down PARP-1 (*HCT116 siPARP1*) or control (*HCT116 siCont*) cells were mock-transfected or transfected with FLAG-CHFR expression vectors. Twenty-four hours after transfection, the cells were treated with 0.5 μM docetaxel for 16 h, and the MI was determined (*right panel, bottom*). Experiments were performed in triplicate. The mean ± S.D. is indicated by *bars* and *brackets*, respectively. *p* values were calculated using Student's *t* test. The cell lysates were examined by immunoblotting with each of antibodies against the indicated proteins (*top panel*).

Ub-proteasome system in response to various stimuli. Indeed, previous work has shown that PARP-1 is subject to ubiquitination and proteasome-dependent degradation in response to DNA damage and heat shock (22, 23). Thus, we sought to determine whether CHFR expression correlated with PARP-1 expression levels during mitotic stress. As shown in Fig. 3*C*, overexpression of CHFR decreased PARP-1 protein levels in HCT116 and HCS-44 cells, which do not express endogenous CHFR, and mitotic stress induced by nocodazole promoted the degradation of PARP-1, suggesting that CHFR promotes polyubiquitination and degradation of PARP-1 in response to mitotic stress. In agreement with these data, MEFs prepared from *Chfr* KO mice had higher levels of PARP-1 protein compared with MEFs from *Chfr* WT mice, even though there was no significant difference in *Parp1* mRNA expression between WT and KO MEFs (Fig. 3*D*). As reported previously, Aurora A and Plk-1, which were polyubiquitination substrates of CHFR, were also overexpressed in *Chfr* KO MEFs (1). Moreover, in *Chfr* WT MEFs, PARP-1 protein accumulated with MG132 treatment (Fig. 3*D*, *lanes 1* and *3*) and decreased with docetaxel treatment, a microtubule inhibitor (*lanes 1* and *5*). Interestingly, the decrease in PARP-1 protein expression induced by docetaxel was inhibited by the concomitant use of MG132 (Fig. 3*D*, *lanes 5* and *7*). The polyubiquitination of PARP-1 in *Chfr* WT MEFs was greater than in KO MEFs, supporting that PARP-1 was mainly polyubiquitinated by CHFR. Moreover, MG132 single treatment promoted the polyubiquitination of PARP-1 in both WT and KO MEFs, whereas combination of MG132 and docetaxel significantly increased only in WT MEFs, favoring the idea that PARP-1 was

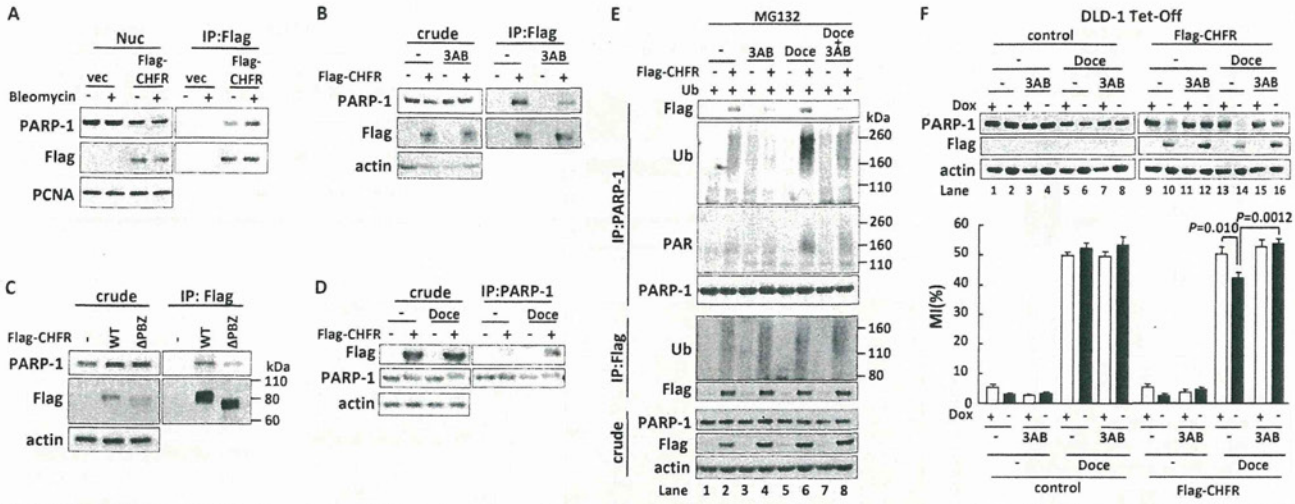

FIGURE 4. **PARP-1 poly(ADP-ribosyl)ates CHFR and regulates the mitotic checkpoint.** *A*, HEK-293T cells were mock-transfected or transfected with FLAG-CHFR expression vectors. After transfection for 24 h, the cells were treated for 18 h with 50 μg/ml of bleomycin or DMSO. Nuclear extracts were immunoprecipitated (*IP*) with an anti-FLAG antibody. The precipitates were examined by immunoblotting with each of antibodies against the indicated proteins. *B*, HCT116 cells were mock-transfected or transfected with a FLAG-CHFR expression vector. After transfection for 24 h, the cells were treated for 16 h with 3 mM 3AB or DMSO. The cell lysates were coimmunoprecipitated with an anti-FLAG antibody, and the precipitates were examined by immunoblotting with each of antibodies against the indicated proteins. *C*, HCT116 cells were mock-transfected or transfected with FLAG-CHFR or FLAG-CHFR ΔPBZ expression vectors. The cell lysates were immunoprecipitated with an anti-FLAG antibody. The precipitates were examined by immunoblotting with each of antibodies against the indicated proteins. *D*, HCT116 cells were mock-transfected or transfected with a FLAG-CHFR expression vector. After transfection for 24 h, the cells were treated for 12 h with 1 μM docetaxel or DMSO (-), and 10 μM MG132 was added following 4 h of incubation. The cell lysates were immunoprecipitated with anti-PARP-1 following immunoblotting with each of antibodies against the indicated proteins. *E*, HCT116 cells were mock-transfected or transfected with ubiquitin (*Ub*) or FLAG-CHFR expression vectors. After transfection for 24 h, the cells were treated for 12 h with 1 mM 3AB, 1 μM docetaxel, or DMSO (-), and 10 μM MG132 was added following 4 h of incubation. The cell lysates were immunoprecipitated with each of antibodies against the indicated proteins. *F*, DLD-1 Tet-Off cells expressing inducible FLAG-CHFR (*FLAG-CHFR*) or mock (*control*) were cultured for 24 h with or without 0.1 μg/ml of doxycycline (*Dox*) (*left panel*) and treated for 16 h with 3 mM 3AB, 1 μM docetaxel (*Doce*), or DMSO, and the MI was determined. The cell lysates were examined by immunoblotting with antibodies against each of the indicated proteins. Experiments were performed in triplicate. The mean ± S.D. is indicated by *bars* and *brackets*, respectively. *p* values were calculated using Student's *t* test.

polyubiquitinated by CHFR in responding to mitotic stress, although other E3 ligases could target PARP-1. Although the birth rate and weight of the *Chfr* KO mice were the same as those of the WT mice, the *Chfr* KO MEFs exhibited a higher growth rate and had an impaired mitotic checkpoint when compared with the WT MEFs (supplemental Figs. S2 and S3 and Table S1). In addition, in primary human gastric cancers, the PARP-1 protein levels were higher in *CHFR*-methylated tissues than in *CHFR*-unmethylated tissues (Fig. 3, *E* and *F*), suggesting that silencing of *CHFR* expression may result in the accumulation of PARP-1 protein.

As mitotic stress facilitated the degradation of PARP-1 in the presence of CHFR, we hypothesized that PARP-1 was involved in the early mitotic checkpoint. To clarify this, we first generated DLD-1 Tet-Off FLAG-CHFR cells in which FLAG-CHFR expression was induced by removing doxycycline. Subsequently, we transfected PARP-1 siRNAs, a mixture of three duplexes, into DLD-1 Tet-Off FLAG-CHFR cells to knock down PARP-1 expression. The increase in the mitotic index (MI, the percentages of the mitotic cells, indicating the abrogation of the prophase checkpoint) induced by docetaxel treatment was attenuated by FLAG-CHFR induction in the control siRNA-transfected DLD-1 cells (Fig. 3*G*, *left panel*, compare *lanes 5* and *7*), indicating that CHFR is involved in cell cycle arrest at prophase. Conversely, in the PARP-1-depleted cells, FLAG-CHFR expression did not affect the progression of cells into mitosis as indicated by the MI (Fig. 3*G*, *left panel*, *lanes 6* and *8*). Remarkably, the MI decreased from 50 to 40% when PARP-1 was knocked down, even in the absence of CHFR expression (Fig. 3*G*, *left panel*, *lanes 5* and *6*), suggesting that the protein level of PARP-1 was critical for progression into mitosis. To validate these results in a different cell line, we generated HCT116 cells that stably expressed PARP-1 siRNA, transfected FLAG-CHFR into these cells, and obtained similar data (Fig. 3*G*, *right panel*). The increase in the MI upon docetaxel treatment was attenuated by FLAG-CHFR expression in HCT116 siControl cells (Fig. 3*G*, *right panel*, *lanes 3* and *4*). Conversely, in HCT116 siPARP1 cells with PARP-1 stably knocked down, FLAG-CHFR expression was not significantly involved in cell cycle arrest, as indicated by the MI (Fig. 3*G*, *right panel*, *lanes 7* and *8*). Notably, CHFR-dependent degradation of PARP-1 was observed in these two cell lines. Taken together, these data suggest that in response to mitotic stress, CHFR directly polyubiquitinates PARP-1 and is involved in a delay into mitosis via PARP-1 degradation.

Autopoly(ADP-ribosyl)ation followed by CHFR-dependent Degradation of PARP-1 Regulates the Mitotic Checkpoint—As PARP-1 has PARylation activity, we assessed its biological implication to the CHFR-dependent checkpoint function. FLAG-CHFR was transfected into HEK-293T cells, and the cells were stimulated with bleomycin, which is widely used to induce PARP-1 activation. Interestingly, the interaction between FLAG-CHFR and PARP-1 was enhanced by bleomycin treatment (Fig. 4*A*). We assumed that inhibition of PARP-1 PARylation activity would weaken the interaction. To evaluate this assumption, we transfected FLAG-CHFR expression plasmids into HCT116 cells and treated the cells with 3AB, a PARP

inhibitor. As shown in the coimmunoprecipitation, the interaction between FLAG-CHFR and PARP-1 was reduced by 3AB treatment (Fig. 4*B*). Because it has been previously reported that CHFR binds to PAR via its PBZ domain (9), the FLAG-CHFR ΔPBZ mutant was subject to a coimmunoprecipitation assay. As shown in Fig. 4*C*, FLAG-CHFR ΔPBZ interacted with PARP-1 weaker than FLAG-CHFR WT, indicating that the PARylation of PARP-1 enhances this interaction. It was also observed that FLAG-CHFR ΔPBZ retained the ability to bind to PARP-1 (Fig. 4*C*), suggesting that CHFR needs its CR region in addition to the PBZ domain to interact with PARP-1 more stably.

As PARP-1 was polyubiquitinated by CHFR and degraded in response to mitotic stress, we speculated that mitotic stress would induce the PARylation of PARP-1 to promote the binding of PARP-1 to CHFR. PARP-1 could then be polyubiquitinated and degraded by CHFR. To confirm this hypothesis, we first examined whether the interaction between CHFR and PARP-1 was affected in response to mitotic stress. The docetaxel treatment enhanced the interaction between CHFR and PARP-1, indicating mitotic stress promotes the binding of CHFR to PARP-1 (Fig. 4*D*). To further examine if the PARylation and polyubiquitination status of PARP-1 was altered by mitotic stress in a CHFR-dependent manner, HCT116 cells were cotransfected with FLAG-CHFR and Ub expression plasmids, treated with docetaxel with or without 3AB, and subjected to immunoprecipitation with an anti-PARP-1 antibody to quantify the PARylation and polyubiquitination of PARP-1. Exposure to docetaxel increased the autoPARylation and polyubiquitination of PARP-1 in a CHFR-dependent manner (Fig. 4*E*, *lane 6*), whereas these modifications were repressed in the presence of 3AB (*lane 8*). Interestingly, the autoPARylation of PARP-1 was higher in CHFR-expressing cells than in CHFR-non-expressing cells (*lanes 5* and *6*). As shown in Fig. 3*A*, CHFR also catalyzed Lys-63-linked and other polyubiquitinations of PARP-1 that could affect the autoPARylation of PARP-1. Autopolyubiquitination of CHFR was slightly affected by docetaxel and 3AB treatment (Fig. 4*E*, *lanes 4*, *6*, and *8*) in agreement with a previous report (9). Collectively, these data demonstrate that in response to mitotic stress, PARP-1 is subject to autoPARylation, which facilitates its interaction with CHFR. PARP-1 is then polyubiquitinated and degraded by the proteasome pathway.

We next investigated whether the PARylation activity of PARP-1 affected the CHFR-dependent mitotic checkpoint. DLD-1 Tet-Off FLAG-CHFR cells were exposed to docetaxel with or without 3AB treatment. In accordance with Fig. 3, *C*, *D*, and *G*, docetaxel treatment promoted PARP-1 degradation in a CHFR-dependent manner. Conversely, 3AB treatment partially inhibited the degradation of PARP-1 mediated by CHFR (Fig. 4*F*, compare *lanes 10*, *12–14*, and *16*, respectively). There was little impact of docetaxel or 3AB treatment on PARP-1 protein levels in DLD-1 Tet-Off control cells (*lanes 1-8*). To quantify the percentages of cells entering mitosis, the MI was determined. Induction of FLAG-CHFR expression diminished the MI increase by docetaxel in the absence of 3AB (Fig. 4*F*, *lanes 13* and *14*), but not in the presence of 3AB (*lanes 15* and *16*). However, 3AB treatment had no effect on the MI in CHFR non-expressing cells (*lanes 5–8*). These data demonstrate that in CHFR-expressing cells, autoPARylation of PARP-1 triggers its degradation by CHFR, which results in cell cycle arrest, whereas in CHFR-non-expressing cells, autoPARylation does not induce PARP-1 degradation and cells progress into mitosis. When the cells were exposed to a microtubule inhibitor, knocking down PARP-1 contributed to the mitotic checkpoint in a CHFR-independent manner, as shown in Fig. 3*G* (*left panel*, *lanes 6* and *8*; *right panel*, *lanes 7* and *8*). Thus, CHFR is involved in the mitotic checkpoint mainly via polyubiquitination of autoPARylated PARP-1.

PARP Inhibitors Sensitize Cancer Cells with CHFR-dependent Resistance to Microtubule Inhibitor—Cell cycle checkpoint dysfunction is often associated with sensitivity to chemotherapeutic agents (24, 25). Indeed, our previous data have shown that the intact checkpoint function of CHFR is related to resistance to microtubule inhibitors (26), and knocking down *CHFR* sensitizes cancer cells to these anticancer drugs (21). Hence, our present findings that CHFR preferentially polyubiquitinated autoPARylated PARP-1, which was then degraded via the proteasome pathway (Fig. 4*E*) and delayed cells in the mitotic checkpoint, led us to test a combination of PARP inhibitors in *CHFR*-expressing cancer cells that are resistant to microtubule inhibitors. Because *BRCA1/2* and *PTEN* mutations have been found to determine cell sensitivity to PARP inhibitors (16), we chose cancer cells in which mutations in these genes have not been reported. As shown in Fig. 5, the combination of docetaxel and 3AB increased apoptosis in *CHFR* expressing cells, which were resistant to a single treatment with docetaxel. In *CHFR*-silenced cells, the concomitant use of 3AB with docetaxel did not increase apoptosis. These results indicate that the combined usage of PARP and microtubule inhibitors for cancers that are resistant to a single chemotherapy may prove to be beneficial.

DISCUSSION

In this study, we identified PARP-1 as a novel CHFR binding protein and found that the functional relationship between CHFR and PARP-1 regulated CHFR-dependent polyubiquitination and degradation of PARP-1 in response to mitotic stress and then modulated cell cycle arrest at the early mitotic checkpoint. Furthermore, we revealed that the interaction between CHFR and PARP-1 could be regulated by the PARylation activity of PARP-1 (Fig. 6, left). As recent reports have shown that CHFR is an acceptor of PARylation, we also validated PARylation of CHFR by PARP-1 both *in vitro* and in cells (supplemental Fig. S4). Subsequently, CHFR polyubiquitinated autoPARylated PARP-1, and PARP-1 was then degraded by the proteasome system. Strikingly, the reduction in PARP-1 protein levels resulted in prophase cell cycle arrest (Fig. 3*G*), implying that there might be a molecular sensor for the detection of PARP-1 levels for cells to enter and proceed into mitosis. Although historically the focus has been on the role of PARP-1 in DNA damage detection and repair, recent studies have suggested a role for PARP-1 in cell cycle regulation. Several studies have reported that G_2/M arrest is prolonged in PARP-1-deficient cells and that PARP-1 and PARylation are essential for cells entering mitosis, chromosomal condensation, and pro-

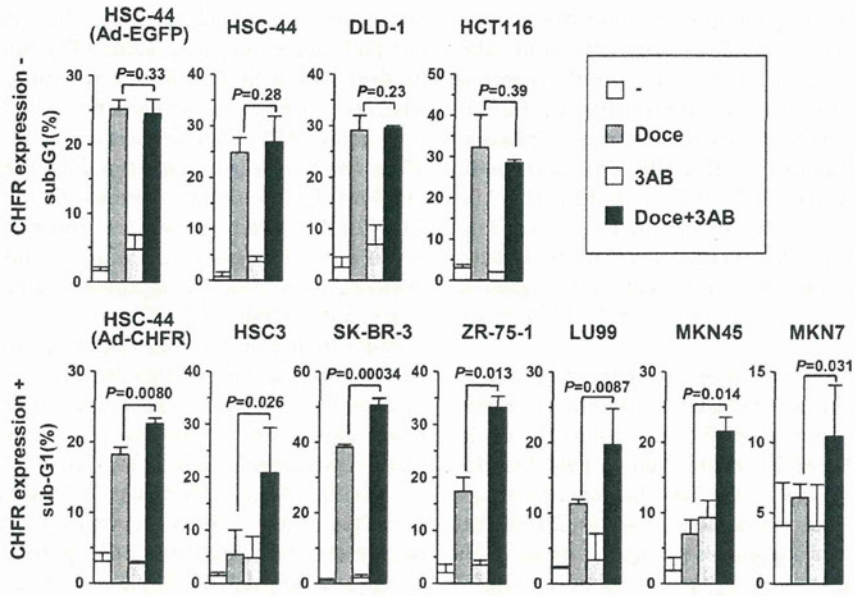

FIGURE 5. **PARP inhibitors sensitize cancer cells with CHFR-dependent resistance to microtubule inhibitors.** One million cells were cultured in 6-mm plates. HCT-44 cells were infected with an adenovirus expressing EGFP (*Ad-EGFP*) or CHFR (*Ad-CHFR*) for 12 h at a multiplicity of infection of 50. The cells were treated for 48 h with 1 μM docetaxel (*Doce*), 10 mM 3AB, or DMSO and subjected to flow cytometry. The percentage of sub-G_1 cells is indicated by the *bars*. Experiments were performed in triplicate. The mean ± S.D. is indicated by *bars* and *brackets*, respectively. *p* values were calculated using Student's *t* test. The original flow cytometry results are indicated in supplemental Fig. S6.

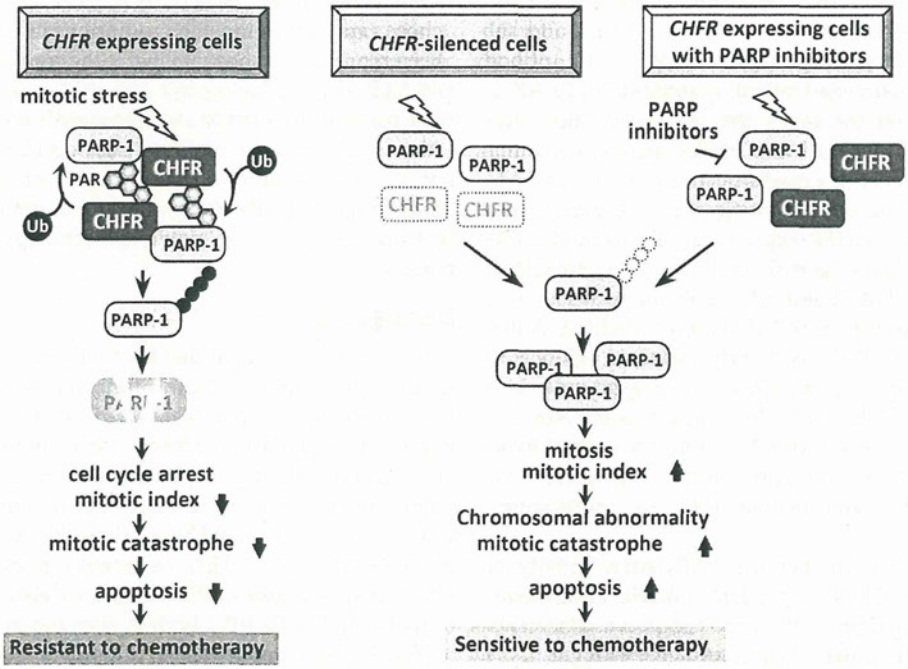

FIGURE 6. **Schematic of the mitotic checkpoint regulated by CHFR and PARP-1 and a cancer therapeutic strategy.** In *CHFR*-expressing cells, mitotic stress induces autoPARylation of PARP-1, which enhances the interaction between CHFR and PARP-1, resulting in an increase in the polyubiquitination/degradation of PARP-1. Decreasing PARP-1 protein levels result in cell cycle arrest at prophase. As shown by our data, cells expressing *CHFR* exhibit resistance to microtubule inhibitors (*left panel*). In CHFR-silenced cells, autoPARylation followed by polyubiquitination of PARP-1 is not induced by mitotic stress. PARP-1 protein expression does not decrease, resulting in the progression of cells into mitosis. Dysfunction of the mitotic checkpoint causes mitotic catastrophe. Consequently, CHFR-silenced cells are sensitive to microtubule inhibitors (*center panel*). In CHFR-expressing cells treated with PARP inhibitors, the autoPARylation of PARP-1 induced by mitotic stress is inhibited by PARP inhibitors. The interaction between CHFR and PARP-1 is diminished, resulting in the repression of CHFR-dependent polyubiquitination/degradation of PARP-1. PARP-1 protein expression does not decrease, resulting in progression into mitosis even in the presence of mitotic stress. Dysfunction of the mitotic checkpoint causes mitotic catastrophe. Therefore, CHFR expressing cells treated with PARP inhibitors are sensitized to microtubule inhibitors (*right panel*).

gression to cell division, implying that PARP-1 would be one of the key mitotic molecules (27–31). Our data suggested that CHFR functioned in cell cycle arrest by decreasing PARP-1 levels before entering mitosis where sufficient amounts of PARP-1 would be required. Previous reports demonstrated that Aurora A and Plk-1 are polyubiquitination substrates of CHFR and